J. Fluid Mech. (2006), *vol.* 557, *pp.* 257–296.
doi:10.1017/S0022112006009724 Printed in the United Kingdom

Inertial effects on the orientation of nearly spherical particles in simple shear flow

By G. SUBRAMANIAN AND D. L. KOCH

Division of Chemical and Bio-molecular Engineering, Cornell University, Ithaca, NY 14853, USA

(Received 15 November 2004 and in revised form 15 April 2005)

We investigate theoretically the first effects of inertia on the orientation dynamics of a torque-free spheroidal particle in simple shear flow when the deviation from sphericity is small. The inertialess motion of any axisymmetric particle in simple shear represents a degenerate limit, the spheroidal geometry being a special case; as originally found by Jeffery (*Proc. R. Soc. Lond.* A, vol. 102, 1922, p. 161), the orientation vector moves indefinitely along any one of a single-parameter family of closed orbits centred around the vorticity axis, the distribution across orbits being determined by initial conditions. We consider both the inertia of the particle and that of the suspending fluid, characterized by the Stokes (St) and Reynolds numbers ($Re = \rho_f/\rho_p St$, ρ_p and ρ_f being the particle and fluid densities), respectively, as mechanisms for breaking the aforementioned degeneracy. The former is defined as $St = a^2\dot{\gamma}\rho_p/\mu$, where $\dot{\gamma}$ is the shear rate, a is the radius of the unperturbed sphere and μ is the fluid viscosity. When the particles are much denser than the suspending fluid, as is the case for aerosols, $St \gg Re$ (both parameters being much less than unity), inertial forces in the fluid may be neglected. It is then found, in the absence of gravity, that a slightly prolate spheroid drifts toward the shearing plane, while the axis of a slightly oblate spheroid tends toward the vorticity axis, both on a time scale of $O(|\epsilon|St\dot{\gamma})^{-1}$, where $\epsilon(\ll 1)$ is the deviation from sphericity. For the case of neutrally buoyant particles ($St = Re$), inertia of both the particle and fluid come into play. In contrast to the small but finite St zero Re case, the orientation vector of a neutrally buoyant prolate spheroid now migrates toward the direction of vorticity, while that of an oblate spheroid drifts towards the shearing plane. The time scale of drift towards the asymptotic state is $O(|\epsilon|Re\dot{\gamma})^{-1}$ in both cases. Thereafter, we also examine the rotations of prolate and oblate spheroids in the presence of both gravity and shear, the analysis again being restricted to weak inertial effects. A wide range of interesting orientational behaviour arises, and the long-time orientation dynamics of the spheroids are determined as a function of both the density ratio ρ_p/ρ_f and a shear parameter N, defined as $N = 2a\rho_f g/(9\mu\dot{\gamma})$.

1. Introduction

Suspensions of solid particles are encountered both as raw materials and intermediates in a large number of industries such as printing and paper-making, petroleum, pharmaceuticals and food processing. In most situations, the particles tend to be non-spherical, or even irregularly shaped, the suspension rheology then being sensitive to the orientation distribution of the suspended particles. The latter is, in turn, affected by several factors including the particle shape and size, the flow conditions, particle–particle interactions etc. In the context of obtaining a

fundamental understanding of such suspension flows, it is therefore of interest to predict the orientation distribution of the particulate phase as a function of the particle properties and flow variables.

The motion of non-spherical particles in shear flows at vanishingly small Reynolds numbers has been studied theoretically for a long time (see Leal 1980). It has, in fact, been known since the work of Jeffery (1922), and later Bretherton (1962), that in the absence of inertia, an axisymmetric particle in a simple shear flow rotates periodically in one of an infinite single-parameter family of closed 'Jeffery' orbits. The particular orbit adopted by the particle, in the absence of hydrodynamic interactions, Brownian motion etc., depends on the initial conditions, however, rendering the inertialess limit indeterminate. In this paper, we consider both particle and fluid inertia as possible mechanisms acting to remove this indeterminacy. The former is characterized by the Stokes number given as $St = a^2\dot{\gamma}\rho_p/\mu$, while the Reynolds number, $Re = a^2\dot{\gamma}\rho_f/\mu$, represents the relative magnitude of fluid inertial and viscous forces; here, a is a typical particle dimension, ρ_p and ρ_f are the particle and fluid densities, $\dot{\gamma}$ is the shear rate, and μ is the fluid viscosity. In order to make analytical progress, we examine the limit where the aforementioned dimensionless parameters are small but finite; thus, the analysis is for the first effects of inertia. The problem is simplified further by assuming the axisymmetric particle to be a spheroid with an aspect ratio close to unity, so the analysis captures the leading-order effect of the deviation from sphericity on the particle orientational motion. Two different cases are investigated herein: the first is that of a massive particle with a much higher density than the fluid for which case St is finite but Re is negligible, a situation characteristic of gas–solid systems, and the second corresponds to a neutrally buoyant particle for which $\rho_p = \rho_f$, or in dimensionless terms, $Re = St$. In each case, we determine the leading-order inertial torque that governs the drift of the spheroidal particle across the inertialess Jeffery orbits. To the order considered, the perturbation remains regular and the inertial torque turns out to be $O(\epsilon St)$ and $O(\epsilon Re)$, respectively, for massive and neutrally buoyant particles; as stated earlier, the deviation from sphericity, ϵ, is assumed to be much less than unity. For all cases examined, the inertial torque eventually moves the particle, on a time scale of $O(|\epsilon|St\dot{\gamma})^{-1})$ (massive) or $O(|\epsilon|Re\dot{\gamma})^{-1})$ (neutrally buoyant), towards a unique steady or periodic state, thereby removing the inertialess degeneracy.

The above analysis for a massive particle in simple shear flow neglects the orienting effects of gravity; in other words, the Reynolds number based on the settling velocity, Re_{sed}, is assumed to be negligible, since a spheroid sedimenting at zero Reynolds number in an otherwise quiescent fluid maintains a constant orientation. The effect of inertia on the orientation of a sedimenting spheroid is known from the work of Cox (1965). Inertial forces arising from the asymmetric finite-Re_{sed} velocity disturbance field cause the spheroid to orient broadside on to the direction of sedimentation. For small deviations from sphericity, the inertial torque is again $O(\epsilon Re_{sed})$ in the limit $Re_{sed} \ll 1$, since the dominant contribution comes from a region around the spheroid of order its own dimension. The regular nature of the inertial contributions in both shear and sedimentation problems allow one, in the limit of weak inertia, to analyse the rotation of a spheroid under the combined effects of sedimentation and shear via a simple superposition. We therefore also investigate the rotation of both prolate and oblate spheroids in the dual limits $Re, Re_{sed} \ll 1$ for varying directions of sedimentation relative to the plane of shear.

In recent years, there has been an increase in the number of studies of particulate suspensions with inertial effects. The dynamics of orientable particles in particular

have been extensively studied using finite-element simulations. Almost all studies in this regard have, however, been restricted to two dimensions owing to computational constraints (Feng & Joseph 1995). In addition, the focus has been more on the motion of particles with a non-spherical cross-section sedimenting in Newtonian and non-Newtonian fluids, rather than their orientation behaviour in shear flows (Feng, Hu & Joseph 1994; Huang, Feng & Joseph 1994; Feng *et al.* 1995). The motion of orientable particles in simple shear flow at finite Reynolds numbers has also been explored using lattice-Boltzmann simulations. Again, these studies, for the most part, examine either two-dimensional problems involving the orientation behaviour of elliptic cylinders, or restricted three-dimensional problems where spheroids are constrained to rotate about one of their principal axes (see Aidun, Lu & Ding 1998; Ding & Aidun 2000). The only three-dimensional lattice-Boltzmann simulations of neutrally buoyant orientable particles in simple shear flow have been carried out by Qi & Luo (2002, 2003) who investigated the rotations of prolate and oblate spheroids in the Reynolds number range $8 < Re < 117$, Re here being defined based on the semi-minor axis. Unlike the inertialess limit, the orientation dynamics in shear flow differ qualitatively in two and three dimensions at finite Reynolds numbers. In the planar case, for instance, the period of rotation of an elliptic cylinder increases with increasing Re, and is found to eventually diverge at a critical Reynolds number via a saddle-node bifurcation. The slowing down of the rotation stems from the presence of recirculating regions on either side of the cylinder that oppose the rotation of the ambient shear flow for any finite Re, eventually arresting it at the critical value Re_c; for an aspect ratio of 2, $Re_c \approx 29$ (Ding & Aidun 2000). The finite-Re orientation behaviour in three dimensions, as delineated by Qi & Luo (2003), is quite distinct. In fact, both prolate and oblate spheroids while exhibiting transitions in the nature of rotation – from tumbling to rolling or vice versa – as a function of Re, do not exhibit a stationary state for the range of Re and aspect ratios examined; the ratio of major to minor axis for all spheroids simulated, both prolate and oblate, was 2. Thus, the negative torque arising due to streamline separation, and the resulting recirculating regions, is presumably never strong enough to stop rotation. Qi & Luo (2003) also found the constraint of a fixed axis of rotation (normal to the plane of shear), imposed by Ding & Aidun (2000) on the ellipsoid, to be an artificial one; at the particular Re, the constrained state is actually an unstable one and does not coincide with the final orientation of a freely rotating oblate spheroid. The simulation results most relevant to the theoretical analysis in this paper are those of Qi & Luo (2003) at the lowest Reynolds numbers. The comparison is made in § 4, wherein possible reasons for the discrepancy are also examined.

The paper is organized as follows. In § 2 we detail our approach, entailing use of the generalized reciprocal theorem (Subramanian & Koch 2005), to obtain an expression for the angular velocity of a torque-free spheroid in simple shear flow at small but finite St or Re. A novel formulation of this theorem allows us, in particular, to relate the $O(Re)$ inertial correction to the angular velocity of a neutrally buoyant spheroid with a near-unity aspect ratio, to the angular velocity of a sphere at small but finite Re. The latter is known from the work of Lin, Peery & Schowalter (1970), and saves us an enormous amount of algebra in the ensuing analysis. The general relation for the inertial angular velocity, derived at the end of § 2, is then used for a massive spheroidal particle (finite St, zero Re) in § 3, and a neutrally buoyant particle (small but finite $Re = St$) in § 4. In the former case, it is found that a prolate spheroid is centrifuged out to a state of equatorial rotation, while an oblate spheroid asymptotes to an axial spin; this orientation behaviour is shown to be generally

true for any axisymmetric particle. For the neutrally buoyant case, inertia of the suspending fluid causes a prolate spheroid to drift toward an axial spin, and an oblate spheroid to tumble, both about the vorticity axis of the ambient simple shear. Recently, Subramanian & Koch (2005) showed, via a reciprocal theorem formulation, that for sufficiently slender bodies in simple shear flow, the first effects of fluid inertia result in a slow $O(Re)$ drift (superposed on the fast Jeffery rotations) toward the flow–gradient plane. The long-time orientation dynamics correspond to a tumbling motion in this plane for $Re < Re_c$, and to a stationary state for $Re > Re_c$, where Re_c is the critical Reynolds number and is a function of the particle aspect ratio. Their results, together with the analysis in § 4, characterize the orientation behaviour for very large and near-unity aspect ratio spheroids, and thus serve to bracket the possible range of behaviour exhibited by a prolate spheroid in simple shear flow, at small Re, as a function of its aspect ratio. In § 5, we also discuss the conclusions of the theoretical analysis in the context of the aforementioned simulations and available, albeit limited, experimental evidence. Then, in § 6, the rotation of a non-neutrally buoyant spheroid is analysed under the combined effects of sedimentation and shear, again in the limit of weak inertia. For gravity aligned along the flow and gradient directions, we find a whole range of interesting orientational motion depending on the relative dominance of sedimentation and shear. Finally, § 7 presents a summary of the results obtained.

2. Method

In order to examine the motion of a spheroidal particle in simple shear, we use a generalization of the well-known reciprocal theorem for Stokes flow (Happel & Brenner 1965). Previously employed in the context of slender fibre motion (see Subramanian & Koch 2005), the generalized reciprocal theorem may be given as

$$\int_S \boldsymbol{n}\cdot\boldsymbol{\sigma}\cdot\tilde{\boldsymbol{u}}\,\mathrm{d}S + \int_V (\nabla\cdot\boldsymbol{\sigma})\cdot\tilde{\boldsymbol{u}}\,\mathrm{d}V = \int_S \boldsymbol{n}\cdot\tilde{\boldsymbol{\sigma}}\cdot\boldsymbol{u}'\,\mathrm{d}S + \int_V (\nabla\cdot\tilde{\boldsymbol{\sigma}})\cdot\boldsymbol{u}'\,\mathrm{d}V, \qquad (2.1)$$

and relates the two sets, $(\boldsymbol{u}', \boldsymbol{\sigma})$ and $(\tilde{\boldsymbol{u}}, \tilde{\boldsymbol{\sigma}})$, of velocity disturbance and stress fields. Here, $\boldsymbol{n}$ is the unit normal pointing into the fluid domain V bounded by the surface S. In applying the reciprocal theorem, the set $(\boldsymbol{u}', \boldsymbol{\sigma})$ corresponds to the motion of the particles being investigated, in our case the rotation of a torque-free spheroid in simple shear for small but finite St (and/or Re), while $(\tilde{\boldsymbol{u}}, \tilde{\boldsymbol{\sigma}})$, a simpler 'test' problem, typically involves motion of the same particle(s) and for which case the solution is known. For a single particle in an unbounded fluid domain, if the velocity disturbance decays sufficiently rapidly away from the particle, the surface integrals at infinity may be neglected, and the bounding surface S in the integrals in (2.1) becomes that of the particle. The particular choice of the test problem is then dictated by the following requirement: the boundary condition satisfied by $\tilde{\boldsymbol{u}}$, or the value of the associated force density $\tilde{\boldsymbol{\sigma}}\cdot\boldsymbol{n}$, on the particle surface be such that one of the surface integrals is directly related to the dynamic quantity of interest, for instance the force on a translating particle, the angular velocity of a torque-free particle in an external flow, etc.

The above approach is exemplified in the work of Subramanian & Koch (2005) who examined the first effects of inertia on the motion of a torque-free fibre in simple shear. Herein, the test problem was chosen as the inertialess rotation of the slender fibre in a quiescent fluid; the surface integral on the left-hand side of (2.1) then

becomes proportional to the torque on the slender fibre in simple shear, being zero for a torque-free fibre, while the one on the right-hand side is proportional to the resulting angular velocity. Along similar lines, one would expect the choice of the test problem for the present case of a spheroid to again be the Stokes rotation of the same particle in a quiescent fluid. While this choice should certainly work, the subsequent evaluations of both the surface and volume integrals become exceedingly tedious. This is because, unlike a fibre for which slender body theory yields tractable expressions for both the velocity disturbance and stress fields at leading order (see Batchelor 1970), the terms in the disturbance velocity field due to a near sphere, arising on account of its deviation (ϵ) from sphericity, have a complicated form even at $O(\epsilon)$ (see Brenner 1964).

In seeking an algebraically less involved approach for analysing a spheroid with aspect ratio close to unity, it is certainly desirable to choose the test problem as one involving a sphere. The surface S in (2.1) still needs to be that of the spheroid in order for the surface integral containing $\boldsymbol{\sigma}$ to be proportional to the torque acting on the spheroid. This then precludes two, perhaps obvious, candidates for the test problem, the first being the Stokes rotation of a solid sphere included within the spheroid. The velocity field due to the inscribed sphere will clearly not satisfy the solid-body rotation condition on the surface of integration S, a spheroidal fluid surface circumscribing the sphere, so that the aforementioned torque relation does not hold. The second one, that of a circumscribing solid sphere rotating in a quiescent fluid, is also not convenient. Though the velocity field for this case satisfies the requirement of solid-body rotation on the surface of an inscribed spheroid, this being the surface S of integration, the surface integral containing $\tilde{\boldsymbol{\sigma}}$ would now entail knowledge of the stress field within the sphere. The difficulty associated with this latter problem is, however, circumvented if the circumscribing sphere were to be a fluid one. We therefore construct a composite velocity field for our test problem with (shear) stress-free solid-body rotation inside a fluid sphere circumscribing the spheroid, and a Stokes rotlet field corresponding to the same angular velocity, outside it (see figure 1). The latter is the velocity disturbance due to a sphere rotating in a quiescent fluid at zero Reynolds number (for instance, see Kim & Karrila 1991); as will be seen later in §4, the inverse-square far-field decay of the rotlet field allows one to determine the inertial torque, to $O(Re)$, on the spheroid in simple shear flow using only the Stokes approximation for the velocity disturbance $\boldsymbol{u}'$. We also note for an incompressible fluid that the velocity field inside the fluid sphere is characterized by an arbitrary constant pressure in the absence of inertia. Such a velocity field is no longer a solution of the Stokes equations because the discontinuity in the shear stress at the surface of the fluid sphere can only be maintained by a surface distribution of forces, and the latter leads to a non-zero divergence for the test stress field $\tilde{\sigma}$. The stress field can, in fact, be written as

$$\tilde{\boldsymbol{\sigma}} = H(r - R_s)\boldsymbol{\sigma}_{rot}, \tag{2.2}$$

where we have taken the pressure inside the fluid sphere of radius R_s to be zero. Here, $H(z)$ is the Heaviside function, and $\boldsymbol{\sigma}_{rot}$ is the stress associated with the rotlet. In equation (2.2) and those that follow, the variables have been made dimensionless using a, the half-length of the spheroid measured along its axis of symmetry, as the length scale, and $\dot{\gamma}^{-1}$, $\dot{\gamma}$ being the shear rate, as the relevant time scale; thus, $\boldsymbol{u}' \sim O(\dot{\gamma}a)$, $\boldsymbol{\sigma} \sim O(\mu\dot{\gamma})$, etc. The radius R_s of the circumscribing fluid sphere depends on the functional form used for the spheroidal surface (see below). Using the expression $(\tilde{\boldsymbol{\Omega}} \wedge \boldsymbol{r})/r^3$ for the rotlet field, $\tilde{\boldsymbol{\Omega}}$ being the angular velocity of the fluid sphere,

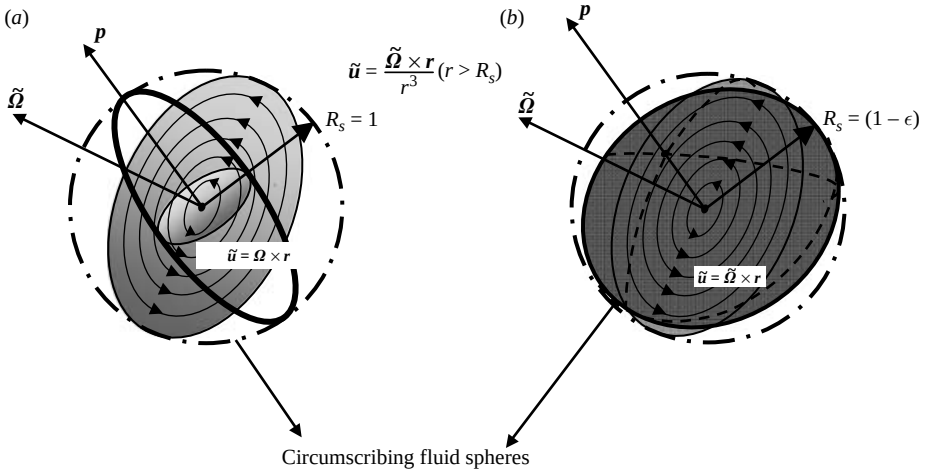

FIGURE 1. The choice of the composite test velocity field $\tilde{\boldsymbol{u}}$ in (2.1) for the cases of (*a*) a prolate and (*b*) an oblate spheroid with axis of symmetry along $\boldsymbol{p}$. It consists of a solid-body rotation field ($\tilde{\boldsymbol{\Omega}} \wedge \boldsymbol{r}$) inside a circumscribing fluid sphere (dot-dashed line) of radius R_s for which the circular streamlines are shown in an equatorial plane; the velocity field in the region $r > R_s$ is a Stokes rotlet field given by $(\tilde{\boldsymbol{\Omega}} \wedge \boldsymbol{r})/r^3$. Note that the prolateness and oblateness have been exagerated for clarity.

(2.2) gives

$$\tilde{\boldsymbol{\sigma}} = -\frac{3}{r^5} H(r - R_s)[(\tilde{\boldsymbol{\Omega}} \wedge \boldsymbol{r})\boldsymbol{r} + \boldsymbol{r}(\tilde{\boldsymbol{\Omega}} \wedge \boldsymbol{r})], \tag{2.3}$$

so that

$$\nabla \cdot \tilde{\boldsymbol{\sigma}} = -\delta(r - R_s) \frac{3(\tilde{\boldsymbol{\Omega}} \wedge \boldsymbol{r})}{r^4}. \tag{2.4}$$

Having made the choice of the test problem, we move on to the problem of interest for which the divergence of the stress field is given by

$$\nabla \cdot \boldsymbol{\sigma} = Re \left[\frac{\partial \boldsymbol{u}'}{\partial t} + \boldsymbol{\Gamma} \cdot \boldsymbol{u}' + (\boldsymbol{\Gamma} \cdot \boldsymbol{r}) \cdot \nabla \boldsymbol{u}' + \boldsymbol{u}' \cdot \nabla \boldsymbol{u}' \right] = \boldsymbol{f}(\boldsymbol{r}), \tag{2.5}$$

where the terms on the right represent the inertial acceleration associated with the disturbance velocity field $\boldsymbol{u}'$ in simple shear for finite Re. Here, $\boldsymbol{\Gamma} = \boldsymbol{e}_x \boldsymbol{e}_y$ is the velocity gradient tensor in simple shear with x, y and z corresponding to the flow, velocity gradient and vorticity directions, respectively.

Using (2.3), (2.4) and (2.5) in (2.1), one obtains

$$\int_S \boldsymbol{n} \cdot \boldsymbol{\sigma} \cdot \tilde{\boldsymbol{u}} \, \mathrm{d}S = -3 \int_{r=R_s} \mathrm{d}S \, (\tilde{\boldsymbol{\Omega}} \wedge \boldsymbol{n}) \cdot \boldsymbol{u}'|_{r=R_s} - Re \int_V \tilde{\boldsymbol{u}} \cdot \boldsymbol{f} \, \mathrm{d}V, \tag{2.6}$$

where the surface element $\mathrm{d}S = R_s^2 \mathrm{d}\hat{S}$, $\mathrm{d}\hat{S}$ being a differential solid angle element. It is seen that the singular force density in the test problem necessitates knowledge of the velocity field $\boldsymbol{u}'$ on the sphere ($r = R_s$) for small but finite Re. Using the solid-body rotation field for $\tilde{\boldsymbol{u}}$ for $r < R_s$ in the surface integral on the left gives

$$\tilde{\boldsymbol{\Omega}} \cdot \mathscr{L} = -3 \int_{r=R_s} \mathrm{d}S \, (\tilde{\boldsymbol{\Omega}} \wedge \boldsymbol{n}) \cdot \boldsymbol{u}'|_{r=R_s} - Re \int_V \tilde{\boldsymbol{u}} \cdot \boldsymbol{f} \, \mathrm{d}V, \tag{2.7}$$

where $\mathscr{L}$ is the non-dimensional torque on the spheroid and V refers to the volume of fluid external to its surface.

For small deviations from sphericity, the surface of a spheroid may be expressed as

$$r = (1 + \epsilon h(\boldsymbol{p}\cdot\boldsymbol{n})) \tag{2.8}$$

with $h(\boldsymbol{p}\cdot\boldsymbol{n}) = (-1 + \boldsymbol{pp}:\boldsymbol{nn}) = -\sin^2\psi$, where ψ is the polar angle made by the unit normal $\boldsymbol{n}$ with the orientation vector $\boldsymbol{p}$ along the spheroidal axis. It is easily seen that the spheroid is prolate for $\epsilon > 0$ and oblate for $\epsilon < 0$; in the former (latter) case, the major and minor axes are $1(1-\epsilon)$ and $1-\epsilon(1)$, respectively. This implies that the radius of the fluid sphere R_s must be 1 for a prolate spheroid and $(1-\epsilon)$ for an oblate one ($\epsilon < 0$), in order for it to circumscribe the spheroid in either case. For finite St, the torque $\mathscr{L}$ on the spheroid is related to its angular acceleration by

$$\mathscr{L} = St\,\frac{\mathrm{d}}{\mathrm{d}t}(\mathscr{I}\cdot\boldsymbol{\Omega}_p), \tag{2.9}$$

where $\boldsymbol{\Omega}_p$ is the angular velocity of the spheroid. In the above, $\mathscr{I} = \mathscr{I}_1\boldsymbol{pp} + \mathscr{I}_2(\boldsymbol{I}-\boldsymbol{pp})$ is the moment of inertia tensor of the spheroid, where the axial and equatorial moments are, respectively, given by $\mathscr{I}_1 = (1-4\epsilon)\mathscr{I}_{sphere}$ and $\mathscr{I}_2 = (1-3\epsilon)\mathscr{I}_{sphere}$ in the limit $\epsilon \ll 1$, $\mathscr{I}_{sphere} = 8\pi/15$ being the non-dimensional moment of inertia of the unperturbed sphere. Using (2.9) and the value of R_s, (2.7), after some manipulation, may be written as

$$St\,\tilde{\boldsymbol{\Omega}}\cdot\left[(\mathscr{I}_1-\mathscr{I}_2)(\boldsymbol{\Omega}_p\cdot\boldsymbol{p})(\boldsymbol{\Omega}_p\wedge\boldsymbol{p}) + \mathscr{I}_2(\boldsymbol{I}-\boldsymbol{pp})\cdot\frac{\mathrm{d}\boldsymbol{\Omega}_p}{\mathrm{d}t} + \mathscr{I}_1\boldsymbol{p}\frac{\mathrm{d}}{\mathrm{d}t}(\boldsymbol{\Omega}_p\cdot\boldsymbol{p})\right]$$
$$= -3\int_{r=R_s}\mathrm{d}S\,(\tilde{\boldsymbol{\Omega}}\wedge\boldsymbol{n})\cdot\boldsymbol{u}'\Big|_{\substack{R_s=1\ (prolate)\\ R_s=1-\epsilon\ (oblate)}} - Re\int_V\tilde{\boldsymbol{u}}\cdot\boldsymbol{f}\,\mathrm{d}V, \tag{2.10}$$

where the left-hand side is identical in structure to the classical Euler's equations for rigid-body rotation (Goldstein 1980). Indeed, on setting the right-hand side in (2.10) to zero, one obtains the dynamics of a torque-free prolate or oblate spheroid in the absence of an ambient flow. Unlike the inertialess limit, the axial spin of the spheroid for finite St affects the equatorial angular momentum balance on account of the centrifugal and gyroscopic mechanisms (see § 3). In the subsequent evaluation of the torque contributions, we use a system of axes that is instantaneously aligned with the spheroidal axis of symmetry $\boldsymbol{p}$, but is fixed in space, so that the ambient simple shear flow is steady in this inertial frame of reference. It is worth mentioning that Euler's equations for rigid-body dynamics, normally derived for a system of body-fixed axes, remain unaltered in this reference frame. This is because the time derivatives in the two frames of reference are related by $(\mathrm{d}/\mathrm{d}t)_{sf}(.) = (\mathrm{d}/\mathrm{d}t)_{bf}(.) + \boldsymbol{\Omega}_p\wedge(.)$, the subscripts sf and bf referring to space-fixed and body-fixed, respectively; the equation for the rate of change of angular velocity thus remains unchanged.

The determination of the inertial angular velocity of a neutrally buoyant spheroid in simple shear (see § 4) requires evaluation of the volume integral on the right-hand side of (2.10). This involves the inertial terms given by $\boldsymbol{f}(\boldsymbol{r})$ in (2.5), and appears to require knowledge of the fluid velocity disturbance $\boldsymbol{u}'$ due to the spheroid at finite Re. As is well-known, determination of a uniformly valid representation of the disturbance velocity field due to particle motions in presence of inertia, and in an unbounded fluid domain, is non-trivial, requiring singular perturbation methods. For the case under consideration, the Stokes approximation to $\boldsymbol{u}'$ breaks down beyond an inertial screening length that scales as $aRe^{-1/2}$, since the convection of $\boldsymbol{u}'$ by the

ambient shear becomes comparable to viscous diffusion at larger distances. Thus, for distances greater than $aRe^{-1/2}$, the 'outer' velocity field must be obtained by solving the linearized Navier–Stokes equation that includes, at leading order, the inertial terms arising from the ambient shear. However, a representation of this outer flow is not needed for our problem since the dominant contributions to the volume integral arise from regions near the particle. To see this simplification we first note that a neutrally buoyant spheroid in a linear flow creates a dipole disturbance velocity that is $O(1/r^2)$ for large distances, and connects smoothly to the outer solution for distances greater than the screening length. The test velocity field due to a rotating sphere has the same far-field dipole character, again being of $O(1/r^2)$ for large r. The contribution to the volume integral from the outer region can then be estimated as

$$\int_{O(Re^{-1/2})}^{\infty} \tilde{\boldsymbol{u}} \cdot \boldsymbol{f}\, \mathrm{d}V \approx \int_{O(Re^{-1/2})}^{\infty} O\left(\frac{1}{r^4}\right) r^2 \mathrm{d}r \sim O\left(Re^{1/2}\right),$$

and affects the angular velocity $\boldsymbol{\Omega}_p$ of the spheroid only at $O(Re^{3/2})$. It therefore suffices to use the Stokes approximation for $\boldsymbol{u}'$ for purposes of determining the first effects of inertia which occur at $O(Re)$. The Stokes velocity disturbance due to an arbitrarily oriented spheroid in simple shear is obtained in § 4 using earlier results of Chwang & Wu (1975).

Finally, we consider the first term on the right-hand side of (2.10) involving the velocity disturbance $\boldsymbol{u}'$ of the spheroid on the surface of the circumscribing fluid sphere $r = R_s$. As was seen earlier, this term is generated by the divergence of the stress $\tilde{\boldsymbol{\sigma}}$ in the test problem, and the relative simplicity of the aforementioned approach is contingent on its evaluation without difficulty. Unlike the case of the volume integral above, there is no prefactor of Re associated with this term, implying that $\boldsymbol{u}'$ must now be determined while accounting for the $O(Re)$ inertial terms. In the limit of the prolate or oblate spheroid having an aspect ratio near unity, i.e. for $\epsilon \ll 1$, one can, however, relate $\boldsymbol{u}'|_{r=R_s}$ to the corresponding disturbance velocity due to a sphere for small but finite Re. In either case, the inertial correction to the Stokes approximation is $O(Re)$, being regular, and entailing a solution of the inhomogeneous Stokes equations in a region near the particle. For the case of a sphere, this has been done previously by Lin, Peery & Schowalter (1970) who examined the first effects of inertia on the rheology of a dilute suspension. In order to use their result, we first note that $\boldsymbol{u}'(\boldsymbol{r}, \boldsymbol{p}, t; \epsilon, Re)$ satisfies the equations

$$\nabla^2 \boldsymbol{u}' - \nabla p = Re\, \boldsymbol{f}(\boldsymbol{r}),$$
$$\nabla \cdot \boldsymbol{u}' = 0,$$

with the boundary conditions

$$\boldsymbol{u}' \to 0 \quad \text{as} \quad r \to \infty,$$
$$\boldsymbol{u}' = (\boldsymbol{\Omega}_p \wedge \boldsymbol{r}) - \boldsymbol{\Gamma} \cdot \boldsymbol{r} \quad \text{at} \quad r = (1 + \epsilon h)\boldsymbol{n}.$$

The boundary condition on the spheroidal surface can be translated onto the surface of a sphere by expanding it as a Taylor series for small ϵ, as is typically done in domain perturbation problems (Leal 1992); we have

$$\boldsymbol{u}'\{(1+\epsilon h)\boldsymbol{n}, \boldsymbol{p}, t; \epsilon, Re\} = \boldsymbol{\Omega}_p \wedge \{(1+\epsilon h)\boldsymbol{n}\} - \boldsymbol{\Gamma} \cdot \{(1+\epsilon h)\boldsymbol{n}\}$$
$$\Rightarrow \boldsymbol{u}'(\boldsymbol{n}, \boldsymbol{p}, t; \epsilon, Re) + \epsilon h \boldsymbol{n} \cdot \nabla \boldsymbol{u}'(\boldsymbol{n}, \boldsymbol{p}, t; \epsilon, Re)$$
$$= (\boldsymbol{\Omega}_p \wedge \boldsymbol{n} - \boldsymbol{\Gamma} \cdot \boldsymbol{n}) + \epsilon h (\boldsymbol{\Omega}_p \wedge \boldsymbol{n} - \boldsymbol{\Gamma} \cdot \boldsymbol{n}) + O(\epsilon^2).$$

Further, writing $\boldsymbol{u}'(\boldsymbol{n}, \boldsymbol{p}, t; \epsilon, Re) = \boldsymbol{u}'^{(0)}(\boldsymbol{n}; Re) + \epsilon \boldsymbol{u}'^{(1)}(\boldsymbol{n}, \boldsymbol{p}; Re) + O(\epsilon^2)$, one obtains

$$O(1) : \boldsymbol{u}'^{(0)}(\boldsymbol{n}; Re) = (\boldsymbol{\Omega}_p \wedge \boldsymbol{n} - \boldsymbol{\Gamma} \cdot \boldsymbol{n}), \tag{2.11}$$

$$O(\epsilon) : \boldsymbol{u}'^{(1)}(\boldsymbol{n}, \boldsymbol{p}; Re) = -h\boldsymbol{n} \cdot \nabla \boldsymbol{u}'^{(0)}|_{r=1} + h(\boldsymbol{\Omega}_p \wedge \boldsymbol{n} - \boldsymbol{\Gamma} \cdot \boldsymbol{n}), \tag{2.12}$$

at successive orders, where the leading-order problem involving $\boldsymbol{u}'^{(0)}$ corresponds to that of a freely rotating sphere in simple shear. Here, we have written down explicitly the dependence of $\boldsymbol{u}'$, $\boldsymbol{u}'^{(0)}$ and $\boldsymbol{u}'^{(1)}$ on both the relevant variables $(\boldsymbol{r}, \boldsymbol{p}, t)$ and parameters (ϵ, Re) in order to emphasize the fact that the leading-order velocity disturbance $\boldsymbol{u}'^{(0)}$ due to a neutrally buoyant sphere in simple shear is time independent. In fact, even $\boldsymbol{u}'^{(1)}$ is dependent only on the instantaneous orientation; unsteady inertial effects $(\partial \boldsymbol{u}'/\partial t)$ only enter the problem at $O(\epsilon^2)$, the dependence on time being implicit via the changing orientation vector $\boldsymbol{p}$.

For the cases of a prolate and an oblate spheroid with $R_s = 1$ and $(1-\epsilon)$ respectively, the velocity on the surface of the circumscribing fluid sphere, to $O(\epsilon)$, may now be found as

$$\boldsymbol{u}'|_{R_s=1} = \boldsymbol{u}'^{(0)}(\boldsymbol{n}) + \epsilon \boldsymbol{u}'^{(1)}(\boldsymbol{n}) \qquad (\epsilon > 0), \tag{2.13}$$

$$\boldsymbol{u}'|_{R_s=1-\epsilon} = \boldsymbol{u}'^{(0)}(\boldsymbol{n}) + \epsilon \left(\boldsymbol{u}'^{(1)}(\boldsymbol{n}) - \boldsymbol{n} \cdot \nabla \boldsymbol{u}'^{(0)}\right) \qquad (\epsilon < 0), \tag{2.14}$$

with the expression for the normal derivative of $\boldsymbol{u}'^{(0)}$ obtained, to $O(Re)$, from Lin *et al.* (1970). The reciprocal theorem, as given by (2.10), takes the form

$$St\,\tilde{\boldsymbol{\Omega}} \cdot \left[(\mathscr{I}_1 - \mathscr{I}_2)(\boldsymbol{\Omega}_p \cdot \boldsymbol{p})(\boldsymbol{\Omega}_p \wedge \boldsymbol{p}) + \mathscr{I}_2(\boldsymbol{I} - \boldsymbol{p}\boldsymbol{p}) \cdot \frac{\mathrm{d}\boldsymbol{\Omega}_p}{\mathrm{d}t} + \mathscr{I}_1 \boldsymbol{p} \frac{\mathrm{d}}{\mathrm{d}t}(\boldsymbol{\Omega}_p \cdot \boldsymbol{p})\right]$$

$$= -3 \int_{r=R_s} \mathrm{d}S(\tilde{\boldsymbol{\Omega}} \wedge \boldsymbol{n}) \cdot \begin{bmatrix} \boldsymbol{u}'^{(0)}(\boldsymbol{n}) + \epsilon \boldsymbol{u}'^{(1)}(\boldsymbol{n}) \\ \boldsymbol{u}'^{(0)}(\boldsymbol{n}) + \epsilon \left(\boldsymbol{u}'^{(1)}(\boldsymbol{n}) - \boldsymbol{n} \cdot \nabla \boldsymbol{u}'^{(0)}\right) \end{bmatrix} - Re \int_V \tilde{\boldsymbol{u}} \cdot \boldsymbol{f}\, \mathrm{d}V, \tag{2.15}$$

where the top row in the matrix on the right corresponds to a prolate spheroid, and the bottom to an oblate one; here, $\boldsymbol{u}'^{(0)}(\boldsymbol{n})$ and $\boldsymbol{u}'^{(1)}(\boldsymbol{n})$ are given by (2.11) and (2.12), respectively. Since the test velocity $\tilde{\boldsymbol{u}}$ in the volume integral is proportional to $\tilde{\boldsymbol{\Omega}}$, the latter is arbitrary, as must be the case.

We observe here that the leading-order inertial torque, to be found in §§ 3 and 4 below, is $O(\epsilon St)$ and $O(\epsilon Re)$ for the cases of a massive and a neutrally buoyant particle. The regularity with respect to the shape parameter ϵ and particle inertia (St) is to be expected, while the regular nature of the correction due to fluid inertia was demonstrated earlier in this section. In particular, the above implies that there is no orienting torque on a sphere $(\epsilon = 0)$ in simple shear flow even in the presence of inertial forces, as is immediately evident from symmetry; it continues to spin about the vorticity axis. In fact, even the $O(Re)$ correction to this axial spin is related to vortex stretching in the ambient linear flow, and the angular spin thus remains unaltered to $O(Re)$ in simple shear (see Lin *et al.* 1970) for which case $\boldsymbol{\omega} \cdot \boldsymbol{E} = 0$, $\boldsymbol{\omega}$ here being the vorticity vector and $\boldsymbol{E}$ the rate-of-strain tensor. This may be used to simplify (2.15) by first noting that the additional term in the surface integral for an oblate spheroid, proportional to $\epsilon \boldsymbol{n} \cdot \nabla(\boldsymbol{u}'^{(0)})$†, is independent of $\boldsymbol{p}$. Then, on rewriting its integral over the unit sphere as

$$3\epsilon \tilde{\boldsymbol{\Omega}} \cdot \int \boldsymbol{n} \wedge \boldsymbol{n} \cdot \nabla \boldsymbol{u}'^{(0)},$$

† This term arises because the radii R_s of the circumscribing fluid spheres for the prolate and oblate cases differ by ϵ, being 1 in the former case and $1-\epsilon$ for the latter.

it follows that the term does not contribute for $Re = 0$ since the velocity disturbance in this case is linear in $\boldsymbol{E}$, and a surface integral over the unit sphere yields $\boldsymbol{\epsilon} : \boldsymbol{E}$ which, of course, vanishes. For finite Re, excluding terms corresponding to solid-body rotation, the handedness of the cross-product (with $\boldsymbol{n}$) ensures that the only non-vanishing quadratic term in the leading-order inertial correction, after angular integration, is of the form $\boldsymbol{\omega} \cdot \boldsymbol{E}$ which is, however, zero for simple shear. Thus, to $O(Re)$, the term $\epsilon \boldsymbol{n} \cdot \nabla \boldsymbol{u}'^{(0)}$ for an oblate spheroid may be neglected. For similar reasons, one may also take $R_s = 1$ in the surface integral in (2.15) for both prolate and oblate spheroids. It will be seen later in § 4 that fluid inertial corrections to the angular velocities of a prolate and an oblate spheroid in simple shear are identical in magnitude, differing only in sign. Using the expression for the rotlet velocity disturbance $\tilde{\boldsymbol{u}}$, and the fact that $\tilde{\boldsymbol{\Omega}}$ is arbitrary, (2.15) may finally be written as

$$St \left[(\mathscr{I}_1 - \mathscr{I}_2)(\boldsymbol{\Omega}_p \cdot \boldsymbol{p})(\boldsymbol{\Omega}_p \wedge \boldsymbol{p}) + \mathscr{I}_2 (\boldsymbol{I} - \boldsymbol{p}\boldsymbol{p}) \cdot \frac{\mathrm{d}\boldsymbol{\Omega}_p}{\mathrm{d}t} + \mathscr{I}_1 \boldsymbol{p} \frac{\mathrm{d}}{\mathrm{d}t} (\boldsymbol{\Omega}_p \cdot \boldsymbol{p}) \right]$$
$$= -3 \int_{r=1} \mathrm{d}S \boldsymbol{n} \wedge \left\{ \boldsymbol{u}'^{(0)}(\boldsymbol{n}) + \epsilon \boldsymbol{u}'^{(1)}(\boldsymbol{n}) \right\} - Re \int_V \frac{(\boldsymbol{r} \wedge \boldsymbol{f})}{r^3} \, \mathrm{d}V, \quad (2.16)$$

with $\epsilon > 0 (< 0)$ for a prolate (oblate) spheroid. In §§ 3 and 4 below, we use (2.16) in order to evaluate Ω_p for the cases of finite St, zero Re and $St = Re$, respectively.

Zhang & Stone (1998) have previously used a modified reciprocal theorem to determine the force and torque on a nearly spherical particle undergoing small-amplitude translational and rotational oscillations in an otherwise quiescent fluid. They, however, only consider unsteady inertial forces, so the fluid motion satisfies the linear unsteady Stokes equations, and the final form of the reciprocal theorem formulation reduces to a relation between surface integrals; the volume distributions of forcing in the presence of convective inertia do not arise. They similarly exploit the known solutions for a sphere by choosing a test problem that involves an unsteadily translating/rotating sphere. Thus, both the sphere and nearly spherical particle satisfy the unsteady Stokes equations for their case, which is unlike the present scenario where the test velocity field does not involve a solid particle at all. In fact, the non-zero divergence of the stress field in our test problem is related to the discontinuity of the shear stress at the surface of the circumscribing fluid sphere, and bears no relation to the governing equations of motion for the non-spherical particle, where the divergence of the stress arises on account of the $O(Re)$ inertial acceleration.

3. Massive spheroidal particle in simple shear flow: $Re = 0$, $St \ll 1$

Herein, we look at the orienting effects of the inertial torque in simple shear when the spheroidal particle is much denser than the suspending fluid, i.e. $\rho_p \gg \rho_f$. In this limit, particle inertia (St) may play an important role in the orientation dynamics with fluid inertial forces, characterized by Re, still being negligible. An added torque arises in such a situation due to inertia associated with settling under gravity, but is not included here; the effects of inertia, associated with both sedimentation and shear, on the orientation dynamics is considered later in § 6. Thus, setting $Re = 0$ in (2.15) gives

$$St \left[(\mathscr{I}_1 - \mathscr{I}_2)(\boldsymbol{\Omega}_p \cdot \boldsymbol{p})(\boldsymbol{\Omega}_p \wedge \boldsymbol{p}) + \mathscr{I}_2 (\boldsymbol{I} - \boldsymbol{p}\boldsymbol{p}) \cdot \frac{\mathrm{d}\boldsymbol{\Omega}_p}{\mathrm{d}t} + \mathscr{I}_1 \boldsymbol{p} \frac{\mathrm{d}}{\mathrm{d}t} (\boldsymbol{\Omega}_p \cdot \boldsymbol{p}) \right]$$
$$= -3 \int_{r=R_s} \mathrm{d}S \boldsymbol{n} \wedge \left\{ \boldsymbol{u}'^{(0)}(\boldsymbol{n}) + \epsilon \boldsymbol{u}'^{(1)}(\boldsymbol{n}) \right\}, \quad (3.1)$$

where $\boldsymbol{u}'^{(0)}$ is now the Stokes velocity disturbance field due to a freely rotating sphere in simple shear. This is well known (for instance, see Leal 1992), being given by

$$\boldsymbol{u}'^{(0)}(\boldsymbol{r}) = -\frac{\boldsymbol{E}\cdot\boldsymbol{r}}{r^5} - \frac{5}{2}\frac{(\boldsymbol{r}\cdot\boldsymbol{E}\cdot\boldsymbol{r})\boldsymbol{r}}{r^5}\left(1-\frac{1}{r^2}\right), \tag{3.2}$$

so that

$$\boldsymbol{u}'^{(0)}(\boldsymbol{n}) = -\boldsymbol{E}\cdot\boldsymbol{n}, \tag{3.3}$$

$$\boldsymbol{n}\cdot\nabla\boldsymbol{u}'^{(0)} = 4\boldsymbol{E}\cdot\boldsymbol{n} - 5\boldsymbol{n}(\boldsymbol{n}\cdot\boldsymbol{E}\cdot\boldsymbol{n}). \tag{3.4}$$

Using (2.12) and (3.4) to calculate $\boldsymbol{u}'^{(1)}$ in (3.1), one obtains after angular integration:

$$\begin{aligned} St\left[(\mathscr{I}_1-\mathscr{I}_2)(\boldsymbol{\Omega}_p\cdot\boldsymbol{p})(\boldsymbol{\Omega}_p\wedge\boldsymbol{p}) + \mathscr{I}_2(\boldsymbol{I}-\boldsymbol{pp})\cdot\frac{\mathrm{d}\boldsymbol{\Omega}_p}{\mathrm{d}t} + \mathscr{I}_1\boldsymbol{p}\frac{\mathrm{d}}{\mathrm{d}t}(\boldsymbol{\Omega}_p\cdot\boldsymbol{p})\right] \\ = -8\pi\left(1-\frac{3\epsilon}{5}\right)\boldsymbol{\Omega}_p + \frac{8\pi\epsilon}{5}(\boldsymbol{\Omega}_p\cdot\boldsymbol{p})\boldsymbol{p} + 4\pi\left(1-\frac{4\epsilon}{5}\right)\boldsymbol{\epsilon}:\boldsymbol{\Gamma} \\ + \frac{8\pi\epsilon}{5}\boldsymbol{p}\wedge(\boldsymbol{\Gamma}\cdot\boldsymbol{p}) + \frac{32\pi\epsilon}{5}\boldsymbol{p}\wedge(\boldsymbol{E}\cdot\boldsymbol{p}). \end{aligned} \tag{3.5}$$

To begin with, considering (3.5) in the inertialess limit, namely $St=0$, we have

$$-2\left(1-\frac{3\epsilon}{5}\right)\boldsymbol{\Omega}_p + \frac{2\epsilon}{5}(\boldsymbol{\Omega}_p\cdot\boldsymbol{p})\boldsymbol{p} + \left(1-\frac{4\epsilon}{5}\right)\boldsymbol{\epsilon}:\boldsymbol{\Gamma} + \frac{2\epsilon}{5}\boldsymbol{p}\wedge(\boldsymbol{\Gamma}\cdot\boldsymbol{p}) + \frac{8\epsilon}{5}\boldsymbol{p}\wedge(\boldsymbol{E}\cdot\boldsymbol{p}) = 0. \tag{3.6}$$

The axial component of (3.6) is just $\boldsymbol{\Omega}_p\cdot\boldsymbol{p} = (1/2)\boldsymbol{\omega}\cdot\boldsymbol{p}$, implying that the particle spins with an angular velocity commensurate with the component of the ambient vorticity along its axis. The equatorial angular momentum balance, to $O(\epsilon)$, reduces to

$$\boldsymbol{\Omega}_p\cdot(\boldsymbol{I}-\boldsymbol{pp}) = \frac{1}{2}\left[\boldsymbol{\epsilon}:\boldsymbol{\Gamma} + \epsilon\left\{-\frac{1}{5}\boldsymbol{\epsilon}:\boldsymbol{\Gamma} + \frac{2}{5}\boldsymbol{p}\wedge(2\boldsymbol{\Gamma}+4\boldsymbol{E})\right\}\right]\cdot(\boldsymbol{I}-\boldsymbol{pp}). \tag{3.7}$$

In a coordinate system with the '1' direction aligned with the spheroidal axis and the '3' direction chosen to lie in the (x, y)-plane (the plane of shear), one has $\Omega_{p2} = \sin\theta\,\mathrm{d}\phi/\mathrm{d}t$ and $\Omega_{p3} = \mathrm{d}\theta/\mathrm{d}t$, where θ is the angle between the spheroidal axis of symmetry and the direction of ambient vorticity, and ϕ is the dihedral angle between the flow–vorticity plane and the plane containing the spheroidal and vorticity axes. The individual components of (3.7) are then given by

$$\Omega_{p3} = \frac{\mathrm{d}\theta}{\mathrm{d}t} = \epsilon\sin\theta\cos\theta\sin\phi\cos\phi, \tag{3.8}$$

$$-\frac{\Omega_{p2}}{\sin\theta} = \frac{\mathrm{d}\phi}{\mathrm{d}t} = -\frac{1}{2} + \frac{\epsilon}{2}(1-2\sin^2\phi), \tag{3.9}$$

which, on identifying ϵ with $e^2/2$, e being the eccentricity, may readily be verified as being the limit of the well-known Jeffery orbit equations for a spheroid in the limit $e \ll 1$. The Jeffery orbit constant is $C = \tan\theta(1-\epsilon\cos^2\phi)$, and it may indeed be shown using (3.8) and (3.9) that $\mathrm{d}C/\mathrm{d}t$ is zero up to $O(\epsilon)$.

For finite St, the axial component of (3.5) reduces to

$$St\frac{\mathrm{d}}{\mathrm{d}t}(\boldsymbol{\Omega}_p\cdot\boldsymbol{p}) = -\frac{15}{2}\left(\boldsymbol{\Omega}_p\cdot\boldsymbol{p} - \frac{1}{2}\boldsymbol{\omega}\cdot\boldsymbol{p}\right), \tag{3.10}$$

which is again a familiar result. Fluid inertia being neglected, the hydrodynamic torque on the particle is quasi-steady and the axial spin ($\boldsymbol{\Omega}_p \cdot \boldsymbol{p}$) of the spheroidal particle, according to (3.10), relaxes exponentially on a time scale of $O(St\dot{\gamma}^{-1})$ towards its steady-state value. Although the latter differs by $O(\epsilon St)$ from its inertialess value, $(1/2)\boldsymbol{\omega}\cdot\boldsymbol{p}$, this correction is not needed for determining the $O(St)$ correction to the orbit equations for a spheroid. Indeed, the axial spin of the spheroid enters the equatorial balance of angular momentum only in the form $St(\boldsymbol{\Omega}_p \cdot \boldsymbol{p})(\mathscr{I}_1 - \mathscr{I}_2)$, $(\mathscr{I}_1 - \mathscr{I}_2)$ being of $O(\epsilon)$, and for purposes of predicting the drift in orientation, it therefore suffices to assume the spheroidal spin as being equal to its inertialess value.

Taking the difference between (3.5) and the projection of (3.10) along $\boldsymbol{p}$, one obtains the following equation for the equatorial angular velocity components at finite St:

$$St\frac{8\pi}{15}\left[-\epsilon(\boldsymbol{\Omega}_p\cdot\boldsymbol{p})(\boldsymbol{\Omega}_p\wedge\boldsymbol{p})+(1-3\epsilon)(\boldsymbol{I}-\boldsymbol{pp})\cdot\frac{\mathrm{d}\boldsymbol{\Omega}_p}{\mathrm{d}t}\right]$$
$$=-8\pi\left(1-\frac{3\epsilon}{5}\right)\boldsymbol{\Omega}_p+4\pi\left(1-\frac{4\epsilon}{5}\right)\boldsymbol{\epsilon}:\boldsymbol{\Gamma}+\frac{8\pi\epsilon}{5}\boldsymbol{p}\wedge(\boldsymbol{\Gamma}\cdot\boldsymbol{p})$$
$$+\frac{32\pi\epsilon}{5}\boldsymbol{p}\wedge(\boldsymbol{E}\cdot\boldsymbol{p}). \tag{3.11}$$

Expand $\boldsymbol{\Omega}_p$ in the form

$$\boldsymbol{\Omega}_p=\boldsymbol{\Omega}_p^j+St\,\boldsymbol{\Omega}_p^c+\ldots,$$

with $\boldsymbol{\Omega}_p^j$ the inertialess Jeffery value whose equatorial components are given by (3.8) and (3.9), and $\boldsymbol{\Omega}_p^c$ the leading-order inertial correction. At $O(St)$, one obtains

$$\boldsymbol{\Omega}_p^c=-\frac{1}{15}\left[-\frac{\epsilon}{4}(\boldsymbol{\omega}\cdot\boldsymbol{p})(\boldsymbol{\omega}\wedge\boldsymbol{p})+(\boldsymbol{I}-\boldsymbol{pp})\cdot\frac{\mathrm{d}\boldsymbol{\Omega}_p^j}{\mathrm{d}t}\right], \tag{3.12}$$

where we have used the fact that $\boldsymbol{\Omega}_p=\boldsymbol{\omega}/2+O(\epsilon)$, and neglected all terms that are $O(\epsilon^2)$ or smaller.

Substituting for $\boldsymbol{\Omega}_p^j$ and, as before, employing a coordinate system aligned with the spheroidal axis, one obtains

$$\Omega_{p2}^c=\frac{1}{15}\sin\theta\sin\phi\cos\phi, \tag{3.13}$$

$$\Omega_{p3}^c=\frac{-1}{15}\left[-\frac{\cos\theta\sin\theta}{4}+\frac{\sin\theta\cos\theta}{2}(\sin^2\phi-\cos^2\phi)\right], \tag{3.14}$$

where, in (3.14), we have written down separately the angular acceleration arising from the term $(\boldsymbol{\omega}\cdot\boldsymbol{p})(\boldsymbol{\omega}\wedge\boldsymbol{p})$, proportional to the axial spin of the spheroid, and that arising from the variation of its inertialess angular velocity along a Jeffery orbit. The latter turns out to be periodic and therefore does not contribute to a net drift of the spheroidal orientation vector.

To $O(\epsilon St)$, the orbit equations may be written as

$$\frac{\mathrm{d}\theta}{\mathrm{d}t}=\epsilon\sin\theta\cos\theta\sin\phi\cos\phi+\frac{\epsilon St}{30}\sin\theta\cos\theta\left(\frac{1}{2}+(\cos^2\phi-\sin^2\phi)\right), \tag{3.15}$$

$$\frac{\mathrm{d}\phi}{\mathrm{d}t}=-\frac{1}{2}+\frac{\epsilon}{2}(1-2\sin^2\phi)-\frac{\epsilon St}{15}\sin\phi\cos\phi. \tag{3.16}$$

It is seen from (3.16) that the orientation distribution of the inertial spheroid in simple shear is no longer symmetrical about the velocity gradient axis. Specifically,

the finite-St correction causes the spheroid to spend an additional $O(St)$ amount of time in the compressional quadrants, as it (slowly) rotates out of flow alignment, than in the extensional ones.

The equation for the orbit constant, to $O(St\epsilon)$, then becomes

$$\frac{\mathrm{d}C}{\mathrm{d}t} = \sec^2\theta \frac{\mathrm{d}\theta}{\mathrm{d}t}, \tag{3.17}$$

$$\Rightarrow \frac{\mathrm{d}C}{\mathrm{d}t} = \frac{\epsilon St}{30}\left[\frac{1}{2} + (\cos^2\phi - \sin^2\phi)\right] C + O(St\epsilon^2) + O(St^2\epsilon), \tag{3.18}$$

where we have used (3.15) for the change of θ. For a spheroidal aspect ratio close to unity, as is the case for small ϵ, the Jeffery orbits, at leading order, are just circles centred around the vorticity axis, i.e. θ remains constant along one such orbit. This then implies that the change in orbit constant over a 2π rotation, resulting from the second term in (3.18), may simply be calculated as the integral of $(\cos^2\phi - \sin^2\phi)$ over the same interval. This is, of course, zero since the integrand is periodic with a zero mean. Thus, $C \to \infty(0)$ for $\epsilon > 0\,(<0)$; in other words, a prolate spheroid drifts slowly towards the plane of shear over several Jeffery rotations, while the drift of an oblate spheroid is toward the vorticity axis, the drift in either case being entirely due to the first term in (3.18). Figure 2 shows both the orbit of a rotating prolate spheroid, as seen in the (x, y)-plane, with $St = 0.5, \epsilon = 0.5$, and the accompanying increase in the orbit constant (plotted as the renormalized ratio $C/(C+1)$) as a function of time; the rather large values of St and ϵ were deliberately chosen in order to exhibit clearly the tight outward spiralling of the spheroidal axis.

The direction of the drift predicted above appears consistent with the intuitive effect of centrifugal forces acting on prolate and oblate distributions of mass revolving in a (circular) Jeffery orbit. This does not reveal the complete picture, however. For instance, just taking into account this centrifugal mechanism would seem to imply that the only steady-stable orbits of a prolate or an oblate spheroid, in the absence of a suspending fluid, would be rotations about either its axis of symmetry or one of its equatorial axes. Other trajectories, with the angular velocity vector no longer coincident with the spheroidal axis of symmetry, should then spiral out – toward a stable rotation about its equatorial axis for a prolate spheroid, and toward an axial spin for an oblate one. This is, of course, not true, since a torque-free spheroid is known to rotate in a set of non-trivial orbits wherein the angular velocity vector precesses at a constant rate about the fixed angular momentum vector in space. This axisymmetric precession, characterized by the solutions of the Euler equations for rigid-body dynamics, has been extensively documented in classical texts on mechanics (see Goldstein 1980; MacMillan 1960). In order to better understand the inertial drift mechanism for our problem, we therefore start by delineating briefly the physics governing the precessing orbits of a freely suspended spheroid in the absence of an ambient fluid.†

† The necessity of dwelling on what is clearly a thoroughly investigated topic is also motivated by a woeful lack of physical explanations in texts devoted to analytical mechanics. Analyses of rigid-body dynamics usually abound in mathematical details, and ingenious ways of characterizing the properties of the precessing orbits – the latter, in particular, being epitomized by statements like 'the polhode rolls without slipping on the herpolhode lying in the invariable plane' (Goldstein 1980). All of these undoubtedly offer insight into the geometry of precession, but the lack of an accompanying physical picture masks the forces underlying the precession mechanism.

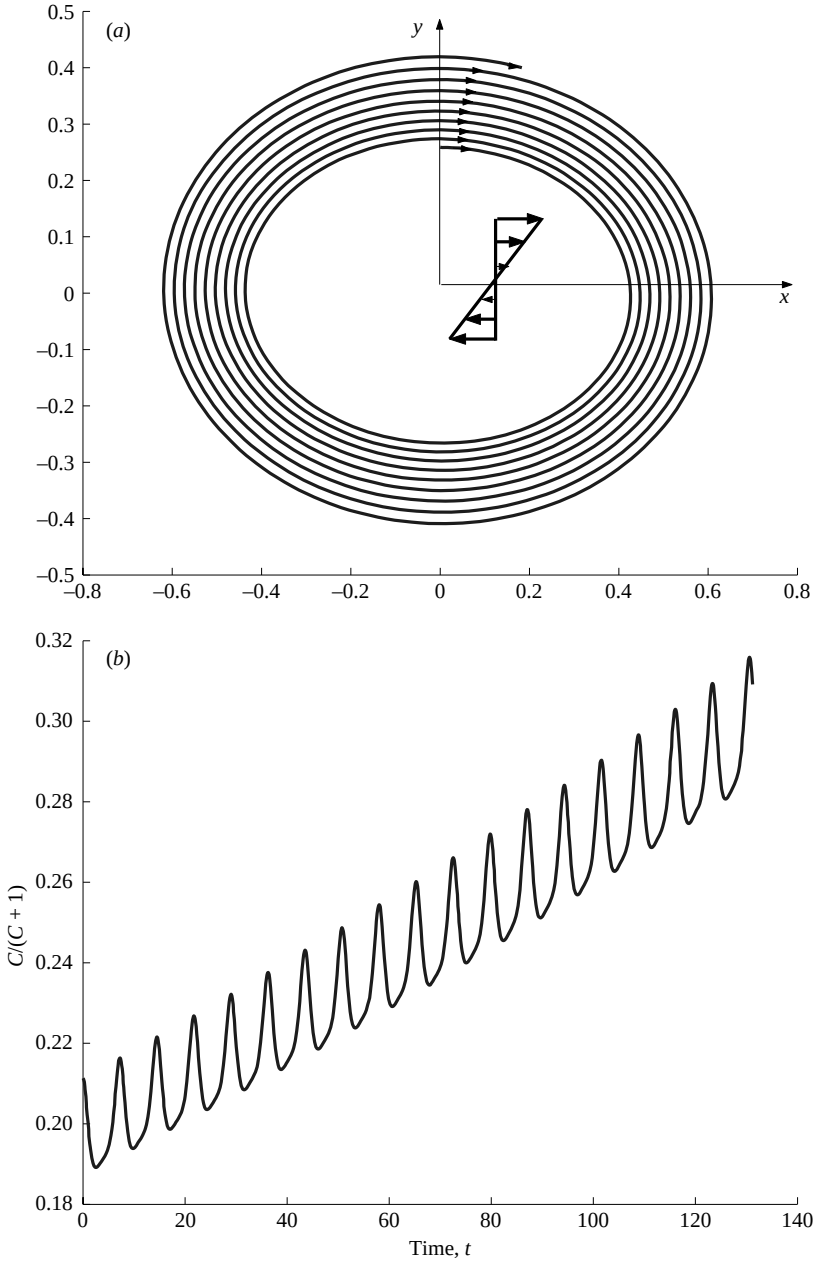

FIGURE 2. (*a*) The orbit, projected onto the flow–gradient plane, of a prolate spheroid in simple shear flow with $Re = 0$, $St = 0.5$ and $\epsilon = 0.5$. The accompanying increase in the orbit constant is shown in (*b*) where the ratio $C/(C+1)$ is plotted as a function of time; note that $C/(C+1) \to 1$ as $t \to \infty$ for a massive prolate spheroid.

The precessions of a prolate and an oblate spheroid are illustrated in figure 3(*a*, *b*), showing them to be the result of a balance between centrifugal and gyroscopic forces. As discussed earlier, the direction of the centrifugal force in the two cases is immediately evident; figure 3(*c*) depicts the details of the gyroscopic force acting on a precessing prolate spheroid. This force commonly manifests itself when one tries to

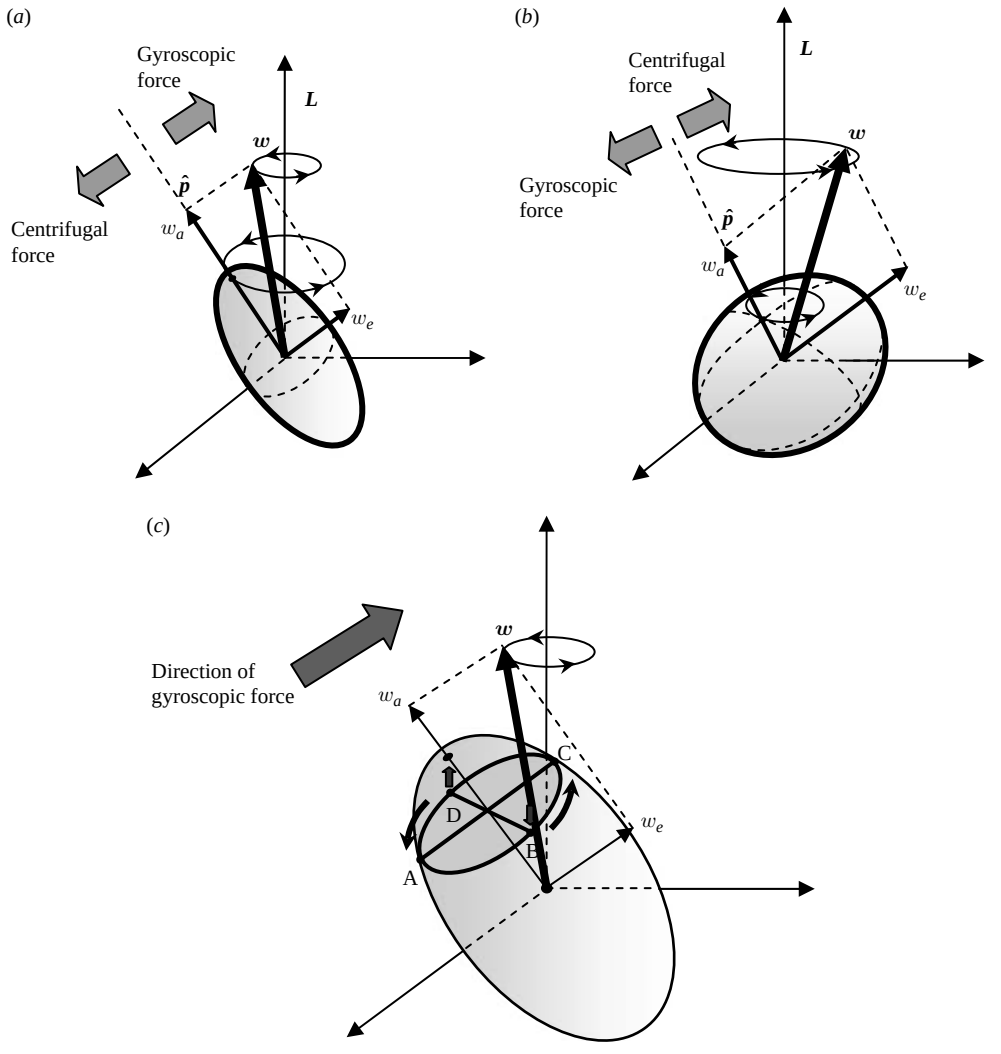

FIGURE 3. (*a*, *b*) The force balance for a torque-free precessing spheroid in (*a*) the prolate and (*b*) oblate cases; here, $\boldsymbol{L}$ denotes the (constant) angular momentum vector, $\boldsymbol{p}$ the axis of symmetry of the spheroid, and $\boldsymbol{\omega}$ the (precessing) angular velocity vector. The (*c*) gyroscopic mechanism that comes into play for a precessing prolate spheroid, and that provides the restoring mechanism opposing the centrifugal forces; refer to text for explanation of symbols.

tilt a spinning wheel; contrary to intuition, the wheel ends up tilting about an axis that is orthogonal to both its spin axis and that corresponding to the applied tilting torque. The gyroscopic mechanism in the context of the precessing spheroid may be understood by decomposing the angular velocity into axial ($\boldsymbol{w}_a$) and equatorial components($\boldsymbol{w}_e$). It is then seen that the plane ABCD, for instance, spins with $\boldsymbol{w}_a$ and is tilted by the equatorial component $\boldsymbol{w}_e$. Focusing on the points B and D, this tilting effect pushes down on the point B and pushes the point D up; however, after a quarter of a spin period, the point B that is being pushed down arrives at C, and the point D goes to A so that the plane ABCD actually tends to tilt in a direction towards the axis of precession $\boldsymbol{L}$. This effect then serves to balance the centrifugal forces tending to push the prolate spheroid out onto its front. It is also evident

then that for this mechanism to act, the axial spin of the prolate spheroid must be faster than that corresponding to solid-body rotation. Since the axial and equatorial angular velocity vectors $\boldsymbol{w}$ add up to a constant in the latter case, the positions of the points A, B, C and D relative to the axis of rotation (also the direction of $\boldsymbol{w}$) remain unchanged; thus, the unbalanced centrifugal forces cause the prolate spheroid to drift towards an equatorial rotation. The greater magnitude of the axial spin component for a precessing prolate spheroid is clearly seen in figure 3 where the angular velocity vector $\boldsymbol{w}$ now tilts towards the spheroidal axis, and itself precesses around the constant angular momentum vector $\boldsymbol{L}$. It immediately follows that the axial spin of an oblate spheroid must be slower than that in a solid-body rotation for the resulting gyroscopic force to balance the centrifugal forces that are now oppositely directed – $\boldsymbol{w}$ again precesses about $\boldsymbol{L}$, but is now located on the opposite side of $\boldsymbol{L}$ relative to $\boldsymbol{p}$ due to the larger relative magnitude of the equatorial component $\boldsymbol{w}_e$.

We now move on to the case of a torque-free spheroid with a near-unity aspect ratio in an ambient fluid subject to simple shear. For small St, the aforementioned forces act on the spheroid as it rotates in an inertialess Jeffery orbit. The Jeffery orbits for a near-sphere are, at leading order, circles centred about the vorticity axis. From (3.8), it is seen, however, that the $O(\epsilon)$ prolate (oblate) deviation from sphericity causes them to be slightly more elongated along the flow (gradient) axis ($\phi = 0(\pi/2)$). The corresponding variation in the angular velocity is so as to make the prolate (oblate) particle rotate more slowly when moving through orientations with ϕ close to $0(\pi/2)$. This $O(\epsilon)$ difference in angular velocity is a periodic fluctuation about the leading-order angular velocity of the sphere. The corresponding additional torque on the near-sphere, due both to the centrifugal and gyroscopic mechanisms, resulting from this periodic angular acceleration will also be periodic with a zero mean, being given by the second term in (3.18), and clearly does not lead to a net drift over a Jeffery period. It therefore suffices, for the purposes of determining the direction of the drift of the spheroid over several rotation cycles, to neglect the $O(\epsilon)$ variation of its angular velocity along a Jeffery orbit. The simplified picture then consists of a prolate or an oblate spheroid executing a solid-body rotation about the vorticity axis, implying that there is no gyroscopic mechanism that can balance the centrifugal forces. The latter, of course, lead to a net drift of any non-axisymmetric distribution of mass. Thus, for small but finite St, a prolate spheroid drifts towards an equatorial rotation (tumbling) in the plane of shear, while the oblate spheroid orientation vector aligns itself with the vorticity direction, consistent with an asymptotic state having only an axial spin. The final simplified picture of a rotating prolate or an oblate spheroid being acted on by centrifugal forces conforms to our earlier intuition.

It is argued now that the above conclusions may, in fact, be extended to a general axisymmetric particle. The aforementioned drift of a prolate or an oblate spheroid may be thought of as being due to centrifugal forces that arise as it rotates in a Jeffery orbit. Now, in the inertialess limit, i.e. with $Re = St = 0$, as shown by Jeffery (1922), any axisymmetric particle rotates indefinitely along a characteristic Jeffery orbit. Also, every such axisymmetric particle has an associated inertia spheroid, representable in terms of a transversely isotropic inertia tensor, that, in the absence of an ambient fluid, would control the free-body dynamics. This inertia spheroid has, of course, the same symmetry axis as the actual body, and therefore the aforementioned mechanism involving centrifugal forces remains unchanged, except that the actual spheroidal particle is now replaced (for the purposes of deducing the drift) by the equivalent inertia spheroid of a generic axisymmetric particle. This immediately leads one to

conclude that the symmetry axis of any prolate (oblate) axisymmetric body will drift towards the plane of shear (vorticity axis) for finite St and zero Re.

4. Neutrally buoyant spheroidal particle in simple shear flow: $Re(=St) \ll 1$

In order to determine the torque on a neutrally buoyant spheroid in simple shear at finite Re, one needs to evaluate the volume integral in (2.16) that accounts for the contributions arising from fluid inertial forces. Using the expression for $\boldsymbol{f}(\boldsymbol{r})$ given by (2.5), this inertial contribution becomes

$$Re \int_V \frac{1}{r^3}\boldsymbol{r} \wedge \left[\frac{\partial \boldsymbol{u}'}{\partial t} + \boldsymbol{\Gamma}\cdot\boldsymbol{u}' + (\boldsymbol{\Gamma}\cdot\boldsymbol{r})\cdot\nabla\boldsymbol{u}' + \boldsymbol{u}'\cdot\nabla\boldsymbol{u}'\right] \mathrm{d}V, \tag{4.1}$$

where V refers to the volume external to the spheroidal particle. As argued earlier in § 2, it suffices, at $O(Re)$, to use the Stokes approximation for $\boldsymbol{u}'$, the non-uniform nature of this leading-order term coming into effect only at $O(Re^{3/2})$. In order to obtain the Stokes velocity disturbance due to a spheroid arbitrarily oriented relative to a simple shear flow, we exploit the results of Chwang & Wu (1975) who used the singularity method in order to derive solutions of the Stokes equations for a range of particle shapes and motions. The details of this derivation are summarized in the Appendix; the final form of the Stokes velocity disturbance due to the spheroid in simple shear, in the limit $\epsilon \ll 1$, may then be written as

$$\boldsymbol{u}' = \boldsymbol{u}'^{s} + 2\epsilon(\boldsymbol{v}_1' + \boldsymbol{v}_2' + \boldsymbol{v}_3' + \boldsymbol{v}_4' + \boldsymbol{v}_5'), \tag{4.2}$$

where $\boldsymbol{u}'^{s}$ is given by (3.2) and

$$\boldsymbol{v}_1' = \sin\theta\cos\theta\sin\phi\cos\phi\left[\frac{65}{42}\boldsymbol{U}_{SS}(\boldsymbol{r};\boldsymbol{p},\boldsymbol{p}_1^{\perp}) + \frac{9}{14}\boldsymbol{p}\cdot\nabla\boldsymbol{U}_D(\boldsymbol{r};\boldsymbol{p}_1^{\perp}) - \frac{1}{6}\boldsymbol{p}\boldsymbol{p}:\nabla\nabla\boldsymbol{U}_{SS}(\boldsymbol{r};\boldsymbol{p},\boldsymbol{p}_1^{\perp}) - \frac{1}{42}\boldsymbol{p}\boldsymbol{p}\boldsymbol{p}\vdots\nabla\nabla\nabla\boldsymbol{U}_D(\boldsymbol{r};\boldsymbol{p}_1^{\perp})\right], \tag{4.3}$$

$$\boldsymbol{v}_2' = \frac{\sin\theta(\cos^2\phi - \sin^2\phi)}{2}\left[\frac{65}{42}\boldsymbol{U}_{SS}(\boldsymbol{r};\boldsymbol{p},\boldsymbol{p}_2^{\perp}) + \frac{9}{14}\boldsymbol{p}\cdot\nabla\boldsymbol{U}_D(\boldsymbol{r};\boldsymbol{p}_2^{\perp}) - \frac{1}{6}\boldsymbol{p}\boldsymbol{p}:\nabla\nabla\boldsymbol{U}_{SS}(\boldsymbol{r};\boldsymbol{p},\boldsymbol{p}_2^{\perp}) - \frac{1}{42}\boldsymbol{p}\boldsymbol{p}\boldsymbol{p}\vdots\nabla\nabla\nabla\boldsymbol{U}_D(\boldsymbol{r};\boldsymbol{p}_2^{\perp})\right], \tag{4.4}$$

$$\boldsymbol{v}_3' = \cos\theta(\cos^2\phi - \sin^2\phi)\left[\frac{20}{21}\boldsymbol{U}_{SS}(\boldsymbol{r};\boldsymbol{p}_1^{\perp},\boldsymbol{p}_2^{\perp}) + \frac{5}{14}\boldsymbol{p}_1^{\perp}\cdot\nabla\boldsymbol{U}_D(\boldsymbol{r};\boldsymbol{p}_2^{\perp}) - \frac{1}{12}\boldsymbol{p}\boldsymbol{p}:\nabla\nabla\boldsymbol{U}_{SS}(\boldsymbol{r};\boldsymbol{p}_1^{\perp},\boldsymbol{p}_2^{\perp}) - \frac{1}{84}\boldsymbol{p}\boldsymbol{p}\boldsymbol{p}_1^{\perp}\vdots\nabla\nabla\nabla\boldsymbol{U}_D(\boldsymbol{r};\boldsymbol{p}_2^{\perp})\right], \tag{4.5}$$

$$\boldsymbol{v}_4' = (\sin^2\theta - 2)\sin\phi\cos\phi\left[\frac{20}{21}\boldsymbol{U}_{SS}(\boldsymbol{r};\boldsymbol{p}_1'^{\perp},\boldsymbol{p}_2'^{\perp}) + \frac{5}{28}(\boldsymbol{p}_2^{\perp}\cdot\nabla\boldsymbol{U}_D(\boldsymbol{r};\boldsymbol{p}_2^{\perp}) - \boldsymbol{p}_1^{\perp}\cdot\nabla\boldsymbol{U}_D(\boldsymbol{r};\boldsymbol{p}_1^{\perp})) - \frac{1}{12}\boldsymbol{p}\boldsymbol{p}:\nabla\nabla\boldsymbol{U}_{SS}(\boldsymbol{r};\boldsymbol{p}_1'^{\perp},\boldsymbol{p}_2'^{\perp}) - \frac{1}{168}\boldsymbol{p}\boldsymbol{p}:\nabla\nabla(\boldsymbol{p}_2^{\perp}\cdot\nabla\boldsymbol{U}_D(\boldsymbol{r};\boldsymbol{p}_2^{\perp}) - \boldsymbol{p}_1^{\perp}\cdot\nabla\boldsymbol{U}_D(\boldsymbol{r};\boldsymbol{p}_1^{\perp}))\right], \tag{4.6}$$

$$\boldsymbol{v}_5' = \frac{\sin^2\theta\sin\phi\cos\phi}{2}\left[\frac{5}{7}\boldsymbol{U}_{SS}(\boldsymbol{r};\boldsymbol{p},\boldsymbol{p}) + \frac{9}{14}\boldsymbol{p}\cdot\nabla\boldsymbol{U}_D(\boldsymbol{r};\boldsymbol{p}) - \frac{1}{4}\boldsymbol{p}\boldsymbol{p}:\nabla\nabla\boldsymbol{U}_{SS}(\boldsymbol{r};\boldsymbol{p},\boldsymbol{p}) - \frac{1}{28}\boldsymbol{p}\boldsymbol{p}\boldsymbol{p}\vdots\nabla\nabla\nabla\boldsymbol{U}_D(\boldsymbol{r};\boldsymbol{p}),\right]. \quad (4.7)$$

Here, we have used $(\boldsymbol{p}, \boldsymbol{p}_1^{\perp}, \boldsymbol{p}_2^{\perp})$ for the unit orthonormal set $(\mathbf{1}_1, \mathbf{1}_2, \mathbf{1}_3)$ in the interests of retaining vector notation; in the latter coordinate system, the unit vector $\mathbf{1}_1$ is aligned with the spheroidal axis, while $\mathbf{1}_3$ is perpendicular to the ambient vorticity vector in simple shear. Thus, $\boldsymbol{p}_1'^{\perp} = (\boldsymbol{p}_1^{\perp} + \boldsymbol{p}_2^{\perp})/\sqrt{2}$ and $\boldsymbol{p}_2'^{\perp} = (\boldsymbol{p}_2^{\perp} - \boldsymbol{p}_1^{\perp})/\sqrt{2}$.

The fluid contribution to the inertial torque on the spheroid is given by

$$Re\int_V \frac{1}{r^3}\boldsymbol{r}\wedge\left[\frac{\partial\boldsymbol{u}'}{\partial t} + \boldsymbol{\Gamma}\cdot\boldsymbol{u}' + (\boldsymbol{\Gamma}\cdot\boldsymbol{r})\cdot\nabla\boldsymbol{u}' + \boldsymbol{u}'\cdot\nabla\boldsymbol{u}'\right]\mathrm{d}V, \quad (4.8)$$

which may be written as

$$Re\int_{V-V_s}\frac{1}{r^3}\boldsymbol{r}\wedge[\boldsymbol{\Gamma}\cdot\boldsymbol{u}'^s + (\boldsymbol{\Gamma}\cdot\boldsymbol{r})\cdot\nabla\boldsymbol{u}'^s + \boldsymbol{u}'^s\cdot\nabla\boldsymbol{u}'^s]\,\mathrm{d}V + 2\epsilon Re\sum_{i=1}^{5}\int_{V_s}\frac{1}{r^3}\boldsymbol{r}\wedge\left[\frac{\partial\boldsymbol{v}_i'}{\partial t} + \boldsymbol{\Gamma}\cdot\boldsymbol{v}_i' + (\boldsymbol{\Gamma}\cdot\boldsymbol{r})\cdot\nabla\boldsymbol{v}_i' + \boldsymbol{u}'^s\cdot\nabla\boldsymbol{v}_i' + \boldsymbol{v}_i'\cdot\nabla\boldsymbol{u}'^s\right]\mathrm{d}V, \quad (4.9)$$

where V_s is the volume external to the circumscribing fluid sphere. As seen above, it suffices to use the leading-order disturbance $\boldsymbol{u}'^s$ when integrating over the $O(\epsilon)$ annular volume $(V - V_s)$ included between the fluid sphere and the spheroid. On the other hand, since $\boldsymbol{\omega}\cdot\boldsymbol{E} = 0$ in simple shear flow, $\boldsymbol{u}'^s$ when integrated over the volume external to the fluid sphere does not lead to a net torque, and has been excluded in the evaluation of the second term in (4.9). For the same reason, there is no contribution to the torque from the $O(\epsilon)$ annular region included between the circumscribing fluid spheres in the prolate and oblate cases, and it suffices, for the purposes of determining (4.9) to $O(\epsilon Re)$, to take $R_s = 1$.

Since the surface of the spheroid is given by $r = (1 + \epsilon h)$ with $h(\boldsymbol{p}\cdot\boldsymbol{n}) = -1 + \boldsymbol{p}\boldsymbol{p}:\boldsymbol{n}\boldsymbol{n}$, the region contributing to the torque in the first term in (4.9) is an annular region with thickness $\epsilon(1 - \boldsymbol{p}\boldsymbol{p}:\boldsymbol{n}\boldsymbol{n})$. Thus, the volume integral may be written in terms of a surface integral over the unit sphere; one obtains

$$Re\int_{V_s-V}\frac{1}{r^3}\boldsymbol{r}\wedge[\boldsymbol{\Gamma}\cdot\boldsymbol{u}'^s + (\boldsymbol{\Gamma}\cdot\boldsymbol{r})\cdot\nabla\boldsymbol{u}'^s + \boldsymbol{u}'^s\cdot\nabla\boldsymbol{u}'^s]\mathrm{d}V, = \epsilon Re\int_{r=1}\mathrm{d}S(1 - \boldsymbol{p}\boldsymbol{p}:\boldsymbol{n}\boldsymbol{n})\boldsymbol{n}\wedge[\boldsymbol{\Gamma}\cdot\boldsymbol{u}'^s + (\boldsymbol{\Gamma}\cdot\boldsymbol{n})\cdot\nabla\boldsymbol{u}'^s + \boldsymbol{u}'^s\cdot\nabla\boldsymbol{u}'^s], \quad (4.10)$$

where $\boldsymbol{u}'^s(\boldsymbol{n})$ and $\nabla\boldsymbol{u}'^s(\boldsymbol{n})$ may be derived using (3.2). The surface integrals involve angular averages over the unit sphere of polyads of the unit normal having the general form $\boldsymbol{n}\boldsymbol{n}\ldots\boldsymbol{n}$. In particular, one needs to evaluate $\int\boldsymbol{n}\boldsymbol{n}\,\mathrm{d}S$, $\int\boldsymbol{n}\boldsymbol{n}\boldsymbol{n}\boldsymbol{n}\,\mathrm{d}S$ and $\int\boldsymbol{n}\boldsymbol{n}\boldsymbol{n}\boldsymbol{n}\boldsymbol{n}\boldsymbol{n}\,\mathrm{d}S$, all of which are appropriate permutations of the unit tensor δ_{ij} (for instance, see Bird *et al.* 1980). Performing the integrations, (4.10) reduces to

$$\frac{8\pi}{15}(\epsilon Re)\boldsymbol{p}\boldsymbol{p}:[\boldsymbol{\epsilon}\cdot(\boldsymbol{\Gamma}\cdot\boldsymbol{E} + \boldsymbol{E}\cdot\boldsymbol{\Omega})], \quad (4.11)$$

where $\boldsymbol{\epsilon}$ is the third-order unit alternating tensor. Using the expression for the elements

of the velocity gradient tensor in the aforementioned particle-aligned coordinate system, one finally obtains

$$\mathbf{1}_3 \cdot \epsilon Re \int_{r=1} \mathrm{d}S(1 - \boldsymbol{pp}:\boldsymbol{nn})\boldsymbol{n} \wedge [\boldsymbol{\Gamma}\cdot\boldsymbol{u}'^s + (\boldsymbol{\Gamma}\cdot\boldsymbol{n})\cdot\nabla\boldsymbol{u}'^s + \boldsymbol{u}'^s\cdot\nabla\boldsymbol{u}'^s] = \epsilon Re\left[\frac{4\pi}{15}(\sin\theta\cos\theta\sin^4\phi + \sin\theta\cos\theta\sin^2\phi\cos^2\phi)\right]. \quad (4.12)$$

Here, and in what follows, we consider only the component along $\mathbf{1}_3$ (or $\boldsymbol{p}_2^{\perp}$ because, as seen earlier in § 3, it is this component of the angular velocity ($=\mathrm{d}\theta/\mathrm{d}t$) that is responsible for the drift across the inertialess Jeffery orbits.

The evaluation of the second term in (4.9) is, of course, much more tedious, as is evident, in particular, from terms of the form $\boldsymbol{u}'^s\cdot\nabla\boldsymbol{v}_i'$ and $\boldsymbol{v}_i'\cdot\nabla\boldsymbol{u}'^s$. We quote below a result for spherical harmonics that allows a considerable simplification of that calculation, however. This result, immediately proven from the orthogonality properties of spherical harmonics (see Hobson 1931), may be stated in its general form as

$$\int_{V_s} r_{i_1}r_{i_2}\ldots r_{i_{n_1}} \frac{\partial^{(n_2)}}{\partial r_{j_1}\partial r_{j_2}\ldots\partial r_{j_{n_2}}}\left(\frac{1}{r}\right)\frac{\partial^{(n_3)}}{\partial r_{k_1}\partial r_{k_2}\ldots\partial r_{k_{n_3}}}\left(\frac{1}{r}\right)\mathrm{d}V = 0, \quad (4.13)$$

provided $n_3 > n_1 + n_2$.

We discuss its application in two instances: in the evaluation of the terms

$$Re\int_{V_s}\frac{1}{r^3}\boldsymbol{r}\wedge\sum_{i=1}^{5}\frac{\partial\boldsymbol{v}_i'}{\partial t}, \quad \text{and} \quad Re\int_{V_s}\frac{1}{r^3}\boldsymbol{r}\wedge\sum_{i=1}^{5}\boldsymbol{\Gamma}\cdot\boldsymbol{v}_i'.$$

Using (A 14) and (A 15) in the Appendix, the following may easily be shown for the singular solutions $\boldsymbol{U}_{SS}$ and $\boldsymbol{U}_D$:

$$(\boldsymbol{U}_{SS})_i = a_j b_k r_i \frac{\partial^2}{\partial r_j\partial r_k}\left(\frac{1}{r}\right), \quad (4.14)$$

$$\frac{\partial^2}{\partial r_l\partial r_m}(\boldsymbol{U}_{SS})_i = a_j b_k\left[\delta_{im}\frac{\partial^3}{\partial r_l\partial r_j\partial r_k}\left(\frac{1}{r}\right) + \delta_{il}\frac{\partial^3}{\partial r_m\partial r_j\partial r_k}\left(\frac{1}{r}\right) + r_i\frac{\partial^4}{\partial r_l\partial r_m\partial r_j\partial r_k}\left(\frac{1}{r}\right)\right], \quad (4.15)$$

$$\frac{\partial}{\partial r_j}(\boldsymbol{U}_D)_i = c_k\frac{\partial^3}{\partial r_i\partial r_j\partial r_k}\left(\frac{1}{r}\right), \quad (4.16)$$

$$\frac{\partial^3}{\partial r_j\partial r_k\partial r_l}(\boldsymbol{U}_D)_i = c_m\frac{\partial^5}{\partial r_i\partial r_j\partial r_k\partial r_l\partial r_m}\left(\frac{1}{r}\right). \quad (4.17)$$

In the light of the above results, it then follows that the minimum order of the spherical harmonics in the $\boldsymbol{v}_i'$ is 2. Since the factor $\boldsymbol{r}/r^3$ in the volume integral is just $-\nabla(1/r)$, a spherical harmonic of the first order†, it then follows from (4.13)

† The order, in this context, refers to the order of the associated surface harmonic. The solid harmonics, of course, have a negative order.

with $n_1 = n_2 = 1$ that for the components of the fluid inertial contribution under consideration, namely terms of the form

$$\int_{V_s} \frac{1}{r^3} \boldsymbol{r} \wedge \partial \boldsymbol{v}_i'/\partial t \quad \text{and} \quad \int_{V_s} \frac{1}{r^3} \boldsymbol{r} \wedge (\boldsymbol{\Gamma} \cdot \boldsymbol{v}_i'),$$

only the terms proportional to $\boldsymbol{U}_{SS}$ in (A 3)–(A 7) contribute; those involving $\nabla \boldsymbol{U}_D$, $\nabla\nabla \boldsymbol{U}_{SS}$ and $\nabla\nabla\nabla \boldsymbol{U}_D$ contain spherical harmonics of the third or higher order, and integrate to zero. With the $\boldsymbol{U}_{SS}$ being the only contribution, the unsteady inertial term

$$\int_{V_s} \frac{1}{r^3} \boldsymbol{r} \wedge \sigma_{i=1}^{5} \partial \boldsymbol{v}_i'/\partial t$$

may, in fact, be shown to be identically zero owing to the antisymmetry of the cross-product. Similar simplifications accrue for the remaining terms in the volume integral too – in particular, the most complicated term in (A 3)–(A 7), that proportional to $\nabla\nabla\nabla \boldsymbol{U}_D$, is also the one expressible in spherical harmonics of the highest order, and consequently, makes no contribution towards the net torque.

Carrying out the integrations, the '3' component of the second term in (4.9), in the particle-aligned coordinate system, reduces to

$$\begin{aligned} Re \sum_{i=1}^{5} \int_{V_s} \frac{1}{r^3} \boldsymbol{r} \wedge \left[\frac{\partial \boldsymbol{v}_i'}{\partial t} + \boldsymbol{\Gamma} \cdot \boldsymbol{v}_i' + (\boldsymbol{\Gamma} \cdot \boldsymbol{r}) \cdot \nabla \boldsymbol{v}_i' + \boldsymbol{u}'^s \cdot \nabla \boldsymbol{v}_i' + \boldsymbol{v}_i' \cdot \nabla \boldsymbol{u}'^s \right] \mathrm{d}V \cdot \boldsymbol{1}_3 \\ = 2\epsilon Re \left[-\frac{32\pi}{21} \sin\theta \cos\theta \cos^2\phi + \frac{83\pi}{36} \sin\theta \cos^3\theta \sin^2\phi \cos^2\phi \right. \\ - \frac{79\pi}{252} \sin^3\theta \cos\theta \sin^2\phi \cos^2\phi + \frac{83\pi}{72} \sin\theta \cos^2\theta \sin\phi \cos^3\phi \\ - \frac{83\pi}{504} \sin\theta \cos^2\theta \sin^3\phi \cos\phi + \frac{599\pi}{504} \sin^3\theta \sin^3\phi \cos\phi \\ \left. - \frac{599\pi}{504} \sin^3\theta \sin\phi \cos^3\phi + \frac{\pi}{36} \sin\theta \cos\theta \right]. \end{aligned} \tag{4.18}$$

Writing down the reciprocal theorem, given in the general from by (2.16), for a neutrally buoyant particle with $St = Re$,

$$\begin{aligned} Re \left[(\mathscr{I}_1 - \mathscr{I}_2)(\boldsymbol{\Omega}_p \cdot \boldsymbol{p})(\boldsymbol{\Omega}_p \wedge \boldsymbol{p}) + \mathscr{I}_2 (\boldsymbol{I} - \boldsymbol{p}\boldsymbol{p}) \cdot \frac{\mathrm{d}\boldsymbol{\Omega}_p}{\mathrm{d}t} + \mathscr{I}_1 \boldsymbol{p} \frac{\mathrm{d}}{\mathrm{d}t} (\boldsymbol{\Omega}_p \cdot \boldsymbol{p}) \right] \\ = -3 \int_{r=1} \mathrm{d}S \boldsymbol{n} \wedge \left\{ (1 + h\epsilon)(\boldsymbol{\Omega}_p \wedge \boldsymbol{n} - \boldsymbol{\Gamma} \cdot \boldsymbol{n}) - h\epsilon \boldsymbol{n} \cdot \nabla \boldsymbol{u}'^{(0)} \right\} - Re \int_V \frac{(\boldsymbol{r} \wedge \boldsymbol{f})}{r^3} \mathrm{d}V, \end{aligned} \tag{4.19}$$

we observe that the only remaining piece of information needed is an expression for $\partial \boldsymbol{u}'^{(0)}/\partial \boldsymbol{n}$, where $\boldsymbol{u}'^{(0)}$ now corresponds to the velocity disturbance, to $O(Re)$, due to a torque-free sphere in simple shear. The $O(Re)$ correction to the Stokes velocity field

for this case has been derived by Peery (1966), and is given by

$$\begin{aligned}
\boldsymbol{u}'^{(0)}_{Re} = {} & \frac{5}{96}\left(-\frac{21}{r^{11}}+\frac{48}{r^{10}}-\frac{63}{r^{9}}+\frac{40}{r^{8}}-\frac{4}{r^{5}}\right)(\boldsymbol{E}:\boldsymbol{r}\boldsymbol{r})^2\boldsymbol{r} \\
& +\frac{1}{288}\left(\frac{70}{r^{9}}-\frac{135}{r^{8}}+\frac{147}{r^{7}}-\frac{50}{r^{6}}-\frac{72}{r^{5}}+\frac{40}{r^{3}}\right)(\boldsymbol{E}:\boldsymbol{r}\boldsymbol{r})(\boldsymbol{\Gamma}\cdot\boldsymbol{r}) \\
& +\frac{1}{288}\left(\frac{70}{r^{9}}-\frac{135}{r^{8}}+\frac{123}{r^{7}}-\frac{50}{r^{6}}+\frac{72}{r^{5}}-\frac{80}{r^{3}}\right)(\boldsymbol{E}:\boldsymbol{r}\boldsymbol{r})(\boldsymbol{\Gamma}^{\dagger}\cdot\boldsymbol{r}) \\
& +\frac{1}{288}\left(\frac{35}{r^{9}}-\frac{135}{r^{8}}+\frac{426}{r^{7}}-\frac{250}{r^{6}}-\frac{96}{r^{5}}+\frac{20}{r^{3}}\right)(\boldsymbol{\Gamma}\cdot\boldsymbol{r})\cdot(\boldsymbol{\Gamma}\cdot\boldsymbol{r})\boldsymbol{r} \\
& +\frac{1}{288}\left(\frac{35}{r^{9}}-\frac{135}{r^{8}}+\frac{234}{r^{7}}-\frac{250}{r^{6}}+\frac{96}{r^{5}}+\frac{20}{r^{3}}\right)(\boldsymbol{\Gamma}^{\dagger}\cdot\boldsymbol{r})\cdot(\boldsymbol{\Gamma}^{\dagger}\cdot\boldsymbol{r})\boldsymbol{r} \\
& +\frac{1}{288}\left(-\frac{10}{r^{7}}+\frac{45}{r^{6}}-\frac{141}{r^{5}}+\frac{50}{r^{4}}-\frac{24}{r^{3}}+\frac{80}{r}\right)\boldsymbol{\Gamma}^{\dagger}\cdot(\boldsymbol{\Gamma}\cdot\boldsymbol{r}) \\
& +\frac{1}{288}\left(-\frac{10}{r^{7}}+\frac{45}{r^{6}}-\frac{69}{r^{5}}+\frac{50}{r^{4}}+\frac{24}{r^{3}}-\frac{40}{r}\right)\boldsymbol{\Gamma}\cdot(\boldsymbol{\Gamma}^{\dagger}\cdot\boldsymbol{r}) \\
& +\frac{5}{288}\left(-\frac{1}{r^{7}}+\frac{6}{r^{6}}-\frac{21}{r^{5}}+\frac{20}{r^{4}}-\frac{4}{r}\right)(\boldsymbol{\Gamma}:\boldsymbol{\Gamma}^{\dagger})\boldsymbol{r}. \qquad (4.20)
\end{aligned}$$

It is seen that (4.20) does not decay for large r, and is therefore incompatible with the free-stream boundary condition at infinity. As mentioned earlier, this necessitates a singular perturbation analysis in order to obtain a uniformly valid velocity field for finite Re.

From (4.19), the '3' component of the equatorial angular momentum balance for finite Re is therefore given by

$$\begin{aligned}
& -\frac{\epsilon Re}{4}\left(\frac{8\pi}{15}\right)\cos\theta\sin\theta+\frac{8\pi}{15}Re(1-2\epsilon)\frac{\mathrm{d}\Omega_{p3}}{\mathrm{d}t} \\
& \quad = -8\pi\left(1-\frac{3\epsilon}{5}\right)\Omega_{p3} \\
& \qquad +8\pi\epsilon E_{12}+\pi\epsilon Re\sin\theta\cos\theta\left(\frac{20}{21}\sin^2\phi\cos^2\phi-\frac{18}{35}\cos^4\phi+\frac{154}{105}\sin^4\phi\right) \\
& \qquad +2\epsilon Re\left[-\frac{32\pi}{21}\sin\theta\cos\theta\cos^2\phi+\frac{83\pi}{36}\sin\theta\cos^3\theta\sin^2\phi\cos^2\phi\right. \\
& \qquad -\frac{79\pi}{252}\sin^3\theta\cos\theta\sin^2\phi\cos^2\phi+\frac{83\pi}{72}\sin\theta\cos^2\theta\sin\phi\cos^3\phi \\
& \qquad -\frac{83\pi}{72}\sin\theta\cos^2\theta\sin^3\phi\cos\phi+\frac{599\pi}{504}\sin^3\theta\sin^3\phi\cos\phi \\
& \qquad \left.-\frac{599\pi}{504}\sin^3\theta\sin\phi\cos^3\phi+\frac{\pi}{36}\sin\theta\cos\theta+\frac{2\pi}{15}\sin\theta\cos\theta\sin^2\phi\right], \qquad (4.21)
\end{aligned}$$

where we have also used (4.12) and (4.18).

As in § 3, we expand Ω_{p3} as a power series in ϵ and Re; the coefficient Ω^c_{p3} representing the leading-order inertial correction, at $O(\epsilon Re)$, is then given by

$$\begin{aligned}\Omega^c_{p3} = \frac{1}{15}\left[\frac{\cos\theta\sin\theta}{4} - \frac{\sin\theta\cos\theta}{2}(\sin^2\phi - \cos^2\phi)\right] \\ + \frac{\sin\theta\cos\theta}{8}\left(\frac{20}{21}\sin^2\phi\cos^2\phi - \frac{18}{35}\cos^4\phi + \frac{154}{105}\sin^4\phi\right) \\ + \frac{1}{4}\left[-\frac{32}{21}\sin\theta\cos\theta\cos^2\phi + \frac{83}{36}\sin\theta\cos^3\theta\sin^2\phi\cos^2\phi\right. \\ - \frac{79}{252}\sin^3\theta\cos\theta\sin^2\phi\cos^2\phi + \frac{83}{72}\sin\theta\cos^2\theta\sin\phi\cos^3\phi \\ - \frac{83}{72}\sin\theta\cos^2\theta\sin^3\phi\cos\phi + \frac{599}{504}\sin^3\theta\sin^3\phi\cos\phi \\ \left. - \frac{599}{504}\sin^3\theta\sin\phi\cos^3\phi + \frac{1}{36}\sin\theta\cos\theta + \frac{2}{15}\sin\theta\cos\theta\sin^2\phi\right], \quad (4.22)\end{aligned}$$

where the first term is identical to the expression for the inertial correction to the angular velocity of a massive particle ($\rho_p \gg \rho_f$), namely (3.14) in § 3. This term in (4.22) then represents the contribution due solely to the inertia of the neutrally buoyant particle; the remaining terms account for inertia of the suspending fluid.

The equation for the change in orbit constant, to $O(Re\epsilon)$, may be written as

$$\frac{\mathrm{d}C}{\mathrm{d}t} = \epsilon Re\sec^2\theta\,\Omega^c_{p3} = (\epsilon Re\,\xi_n)C, \quad (4.23)$$

where ξ_n, the rate of change of orbit constant with $\rho_p = \rho_f$, is given by

$$\begin{aligned}\xi_n(\theta,\phi) = \frac{1}{30}\left(2\cos^2\phi - \frac{1}{2}\right) + \frac{1}{8}\left(\frac{20}{21}\sin^2\phi\cos^2\phi - \frac{18}{35}\cos^4\phi + \frac{154}{105}\sin^4\phi\right) \\ + \frac{1}{4}\left[-\frac{32}{21}\cos^2\phi + \frac{83}{36}\cos^2\theta\sin^2\phi\cos^2\phi - \frac{79}{252}\sin^2\theta\sin^2\phi\cos^2\phi\right. \\ + \frac{83}{72}\cos\theta\sin\phi\cos^3\phi - \frac{83}{72}\cos\theta\sin^3\phi\cos\phi + \frac{599}{504}\frac{\sin^2\theta}{\cos\theta}\sin^3\phi\cos\phi \\ \left. - \frac{599}{504}\frac{\sin^2\theta}{\cos\theta}\sin\phi\cos^3\phi + \frac{1}{36} + \frac{2}{15}\sin^2\phi\right]. \quad (4.24)\end{aligned}$$

For small Re, both C and θ change only by an $o(1)$ amount over a single Jeffery cycle. The direction of the drift at $O(\epsilon Re)$ is therefore determined by the sign of $\bar{\xi}_n(\theta) = (1/2\pi)\int_0^{2\pi}\xi_n(\theta,\phi)\mathrm{d}\phi$, the rate of change averaged over a Jeffery rotation; here, we have replaced the temporal average by an average over the phase ϕ, since the angular velocity $\mathrm{d}\phi/\mathrm{d}t$ is constant at leading order. Using (4.24), it is easily found that

$$\bar{\xi}_n(\theta) = \left(-\frac{4051}{40320} + \frac{55}{672}\cos^2\theta\right), \quad (4.25)$$

which is negative for all values of θ. Thus, for $\epsilon > 0 (< 0)$, $C \to 0(\infty)$, i.e. a neutrally buoyant prolate spheroid drifts towards the vorticity axis for small but finite Re, while an oblate spheroid does the opposite. Figure 4 depicts the trajectory of the orientation vector of an oblate spheroid, with $\epsilon = -0.15$ and $Re = 0.2$, as it spirals out toward the flow–gradient plane. The outward spiralling is extremely tight for the given parameters, with the resultant curve being almost space-filling on the scale of the plot; a magnified view of the same curve, that includes the initial point, confirms

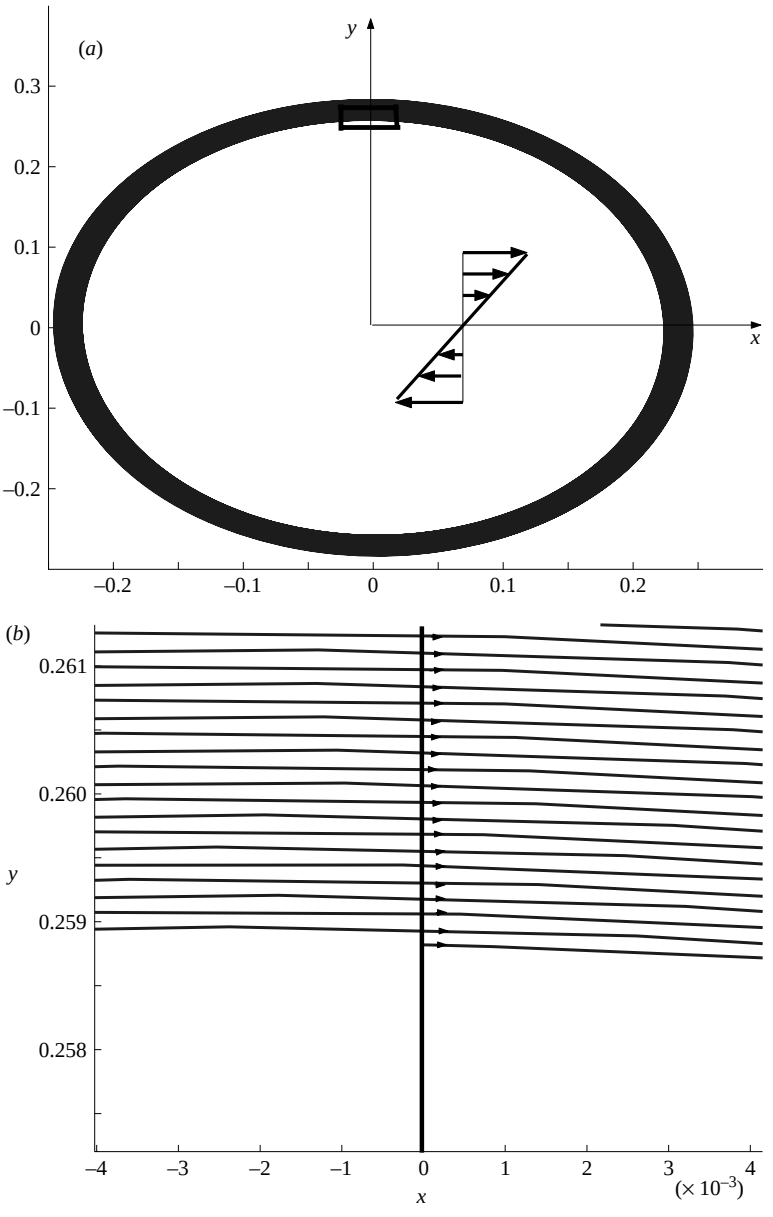

FIGURE 4. (*a*) The orbit, projected onto the flow–gradient plane, of a neutrally buoyant oblate spheroid in simple shear flow with $Re = 0.2, \epsilon = -0.15$. The region marked by the rectangle is then magnified in (*b*) and confirms the nature of the spiralling trajectory.

the nature of spiralling. Figure 5 shows a plot of the accompanying increase in the normalized orbit constant $C/(C+1)$. Note that the oscillations in the orbit constant, on the scale of a single Jeffery cycle, will not be captured in the equation for the average drift characterized by (4.25)†. The above plots were generated by accounting

† The truncation of the non-spherical corrections, at $O(\epsilon)$, itself leads to a spurious oscillation in the orbit constant at $O(\epsilon^2)$; this, however, turns out to be smaller than the oscillations induced by inertial forces.

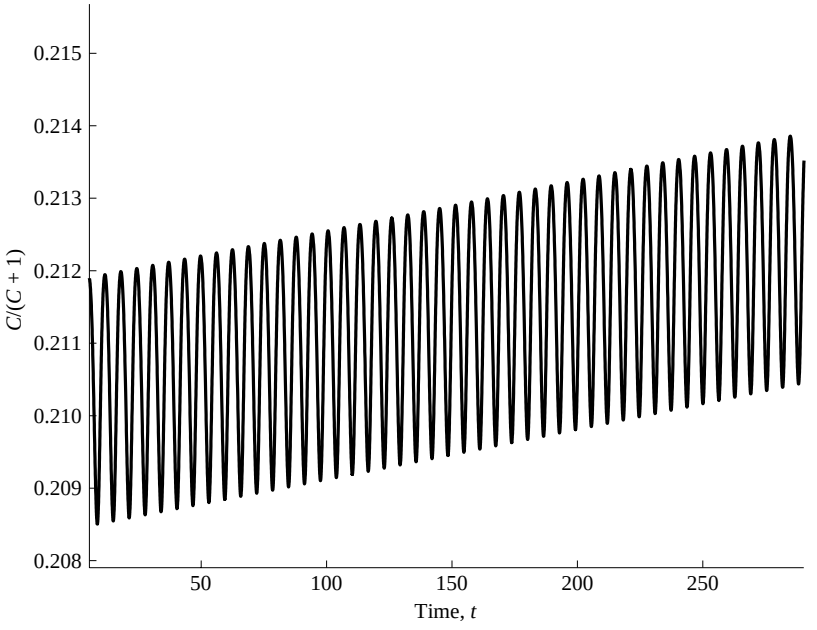

FIGURE 5. The increase in the normalized orbit constant $C/(C+1)$ with time, as an oblate spheroid with $\epsilon = -0.15$ spirals out toward the flow–gradient plane for $Re = 0.2$. Note that $C/(C+1) \to 1$ ($C \to \infty$) as $t \to \infty$ for an oblate spheroid with $\rho_p = \rho_f$.

for the $O(\epsilon Re)$ correction, given by (4.22), contributing to the change in the polar angle θ. The phase equation used for $\mathrm{d}\phi/\mathrm{d}t$ is only correct to $O(\epsilon)$; we do not calculate Ω^c_{p3}, since quantitative alterations in the phase at $O(\epsilon Re)$ do not affect the direction of drift.

Before proceeding to include the orienting effects of gravity in § 6, we note that although the analysis above, and that in § 3, neglected gravity, they were also restricted to considering two limiting situations where $\rho_p = \rho_f$ and $\rho_p \gg \rho_f$. The leading-order inertial drift in the respective cases causes the axis of a prolate spheroid, for instance, to align with the vorticity axis or the flow–gradient plane. With a decrease in the density ratio ρ_p/ρ_f, one then anticipates the long-time orientation behaviour of a prolate spheroid to change from a tumbling motion in the flow–gradient plane to a 'log-rolling' one about the vorticity axis; the transition for an oblate spheroid is expected to be of an opposite character. For an arbitrary ratio of particle to fluid densities, or in dimensionless terms, with St/Re arbitrary, one easily obtains that the averaged drift coefficient governing the change in orbit constant, similar to (4.25), is given by

$$\bar{\xi}(\theta) = \frac{St}{60} + Re\left(-\frac{4723}{40320} + \frac{55}{672}\cos^2\theta\right) \tag{4.26}$$

in the dual limit $St, Re \ll 1$, the contributions due to the inertia of the particle and the suspending fluid now being scaled by St and Re, respectively. Therefore, the polar angle of a possible neutral orbit is given by

$$\theta_n = \cos^{-1}\sqrt{\frac{1}{55}\left(-\frac{56St}{5Re} + \frac{4723}{60}\right)}, \tag{4.27}$$

implying that $\theta_n = \pi/2$ for $St/Re \geqslant 7.028$, and $\theta_n = 0$ for $St/Re \leqslant 2.12$, these, of course, being consistent with results obtained earlier in that the flow–gradient plane and vorticity axis, respectively, act as attractors in the limit $St \gg Re$ and for $St = Re$. The possibility of a steady orbit intermediate between the shearing plane and the direction of vorticity is seen to exist only in the range of density ratios $2.12 < \rho_p/\rho_f (= St/Re) < 7.028$. For this neutral orbit to represent a possible long-time solution for the spheroidal orientation, it must, in addition, be stable. Now, since the drift toward the vorticity axis, given by (4.25), is a decreasing function of θ, this neutral orbit would be stable for a prolate spheroid ($\epsilon > 0$) and unstable for an oblate one ($\epsilon < 0$). In the former case for $\theta < \theta_n$, $(\epsilon\bar{\xi})$ is positive, causing the orientation vector $\boldsymbol{p}$ to migrate in the direction of higher C, and thence back towards the neutral orbit; with $\theta > \theta_n$, the situation is reversed. For an oblate spheroid, the unstable neutral orbit divides the unit sphere into two basins of attraction corresponding to periodic and fixed-point asymptotic states coincident, respectively, with the flow gradient plane and the vorticity axis. As was seen earlier, the tight nature of the spiralling in the limit $\epsilon, Re \ll 1$ makes it difficult to extract information from a plot of the actual trajectory. It is therefore more convenient to represent the orientation dynamics in terms of the normalized orbit constant as is done in figures 6 and 7 for a prolate and oblate spheroid, respectively. The orientation behaviour is shown for a density ratio of 3.5, and the attracting and repelling nature of the neutral orbit may be inferred in the appropriate instances. A change in stability of the neutral orbit in going from a prolate to an oblate deviation from sphericity causes the transitions in orientation behaviour, as a function of the density ratio, for the two cases to no longer be opposite in character.

5. Comparison with previous work

Saffman (1956) seems to have been the first to analyse the motion of a neutrally buoyant spheroid in simple shear flow for small but finite Re. He derived, in effect, an equation for the change in $\bar{C}$, the orbit constant averaged over a complete Jeffery rotation; the final result, in our notation, takes the form

$$\frac{\mathrm{d}\bar{C}}{\mathrm{d}t} = -0.24\epsilon Re\bar{C}. \tag{5.1}$$

As noted earlier, the change in C over a single Jeffery period is $o(1)$, and it therefore makes sense to compare the above prediction to (4.23) with ξ_n replaced by $\bar{\xi}_n$. While both (5.1), and (4.23) modified to include $\bar{\xi}$, predict the asymptotic approach of a prolate (oblate) spheroid towards the vorticity axis (flow–gradient plane), the averaged drift in the former is independent of the polar angle θ. Even the magnitude of the predicted drift is at least twice as large; for instance, $\bar{\xi}_n(\theta)$ in (4.25) tends to its most negative value at $\theta = \pi/2$, this being approximately -0.1. In the same paper, Saffman also concluded that particle inertia alone, when taken into account, would not lead to any net drift. As demonstrated earlier in § 3, this is certainly not the case. An erroneous prediction in the context of what is clearly a simpler problem from an analytical perspective, leads us therefore to suspect the veracity of Saffman's procedure leading to (5.1). He, in fact, only gave a brief sketch of his method, making any detailed comparison very difficult. From what is stated, it appears that rather than using a reciprocal theorem formulation, he solved for the $O(Re)$ inertial velocity field due to the spheroid using, in essence, a regular perturbation approach, together with an ad-hoc modification of the boundary condition at infinity; the latter is, of course,

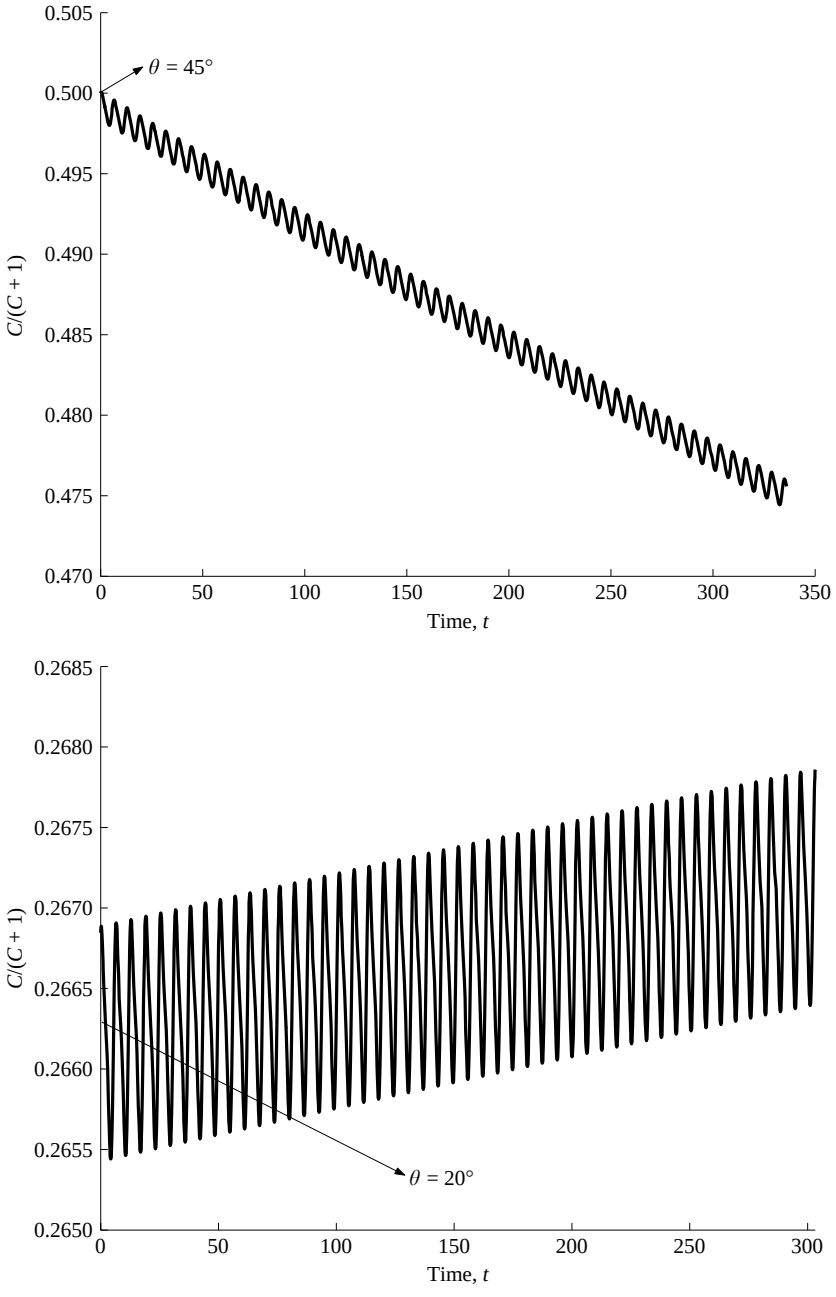

FIGURE 6. Plots of the normalized orbit constants for orbits lying on either side of the neutral orbit of a prolate spheroid with a density ratio of 3.5, for $St = 3.5$, $Re = 0.35$, and $\epsilon = 0.1$, whence the polar angle of the neutral orbit is found to be approximately 30°. The attracting nature of the neutral orbit is readily evident.

needed in the light of the well-known failure of a regular perturbation expansion for such problems†. Keeping in mind the algebraic complexity accompanying a

† To be fair, it must be mentioned that the singular perturbation approach was discovered in 1957, a year after Saffman's analysis (for instance, see Proudman & Pearson 1957; Kaplun & Lagerstrom 1957).

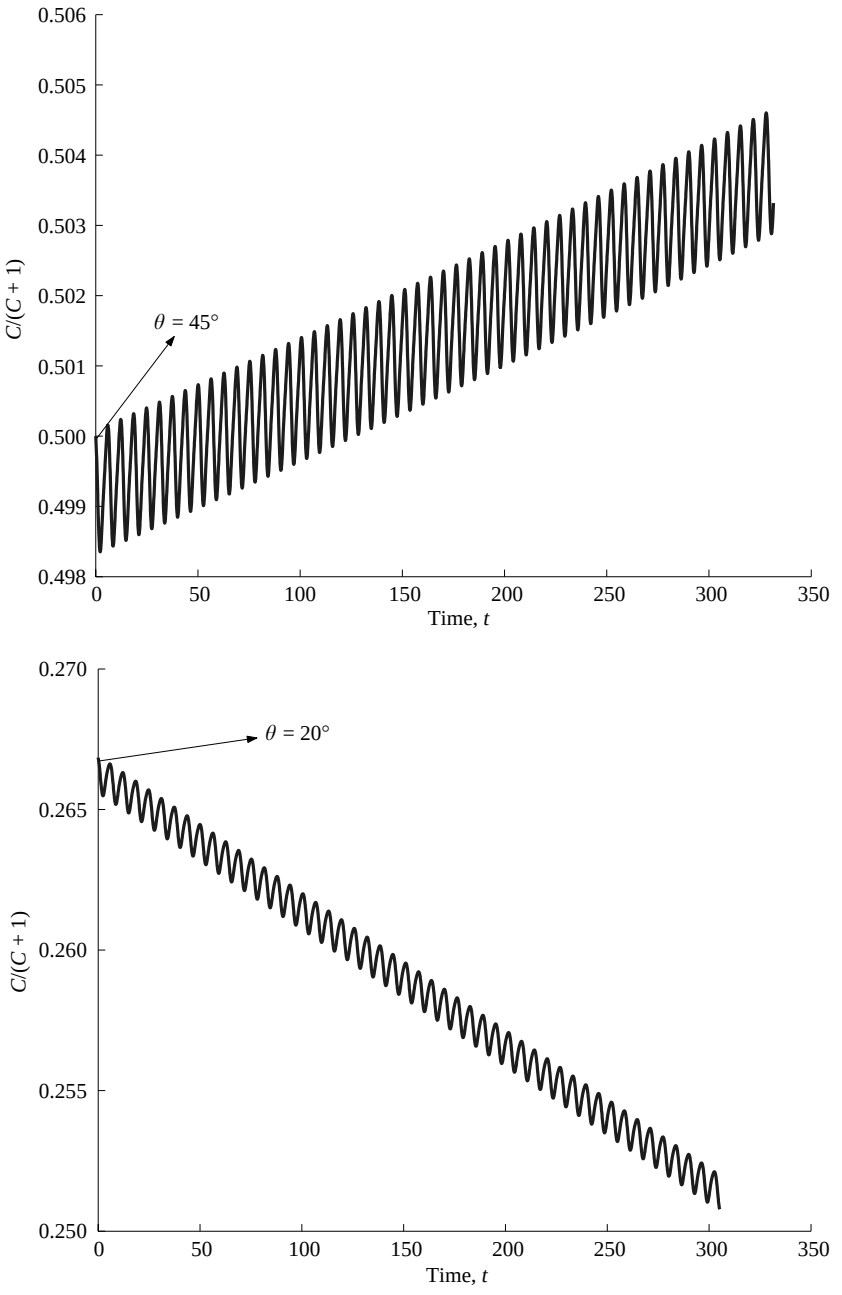

FIGURE 7. Plots of the normalized orbit constants for orbits lying on either side of the neutral orbit of an oblate spheroid with a density ratio of 3.5, for to $St = 3.5$, $Re = 0.35$, and $\epsilon = 0.1$, whence the polar angle of the neutral orbit is found to be approximately 30 degrees. The repelling nature of the neutral orbit is readily evident.

traditional perturbation approach to determining the angular velocity of a neutrally buoyant spheroid, we are inclined to think that Saffman's correct prediction with regard to the direction of spheroidal drift may have been coincidental.

Subramanian & Koch (2005) have calculated the first effects of inertia on the orientational behaviour of slender particles in simple shear flow. They find that inertial

effects lead to a net drift of the slender particle toward the flow–gradient plane. The contrasting orientational behaviour found for neutrally buoyant axisymmetric particles in the limit of large and near-unity aspect ratios suggests a possible bifurcation, entailing a shift of the asymptotic attractor for the orientation vector from the flow–gradient plane to the vorticity axis at an intermediate aspect ratio. We mention below the results of Qi & Luo (2003), which seem to indicate that this critical aspect ratio may not be far from unity. They have examined the orientational behaviour of neutrally buoyant prolate and oblate spheroids, with axis ratios of 2 and 1/2, respectively, in simple shear flow using lattice-Boltzmann simulations for Reynolds numbers ranging from 8 to 117; here, the Reynolds number for the prolate and oblate spheroids is defined based on their semi-major and semi-minor axes, respectively. They found the spheroids to exhibit contrasting behaviour in different ranges of Reynolds numbers. A prolate spheroid 'tumbles', while an oblate spheroid 'rolls' at the lowest Reynolds numbers investigated. For higher Reynolds numbers, both spheroids exhibit a range of intermediate precessing states wherein the mean precession angle between the spheroidal orientation vector and the vorticity axis lies between 0 and $\pi/2$, and decreases (increases) monotonically with increase in the Reynolds number for a prolate (oblate) spheroid. At still higher Reynolds number, the prolate spheroid is found to align itself with the vorticity direction. Thus, although the degeneracy of the Stokes limit is absent in all cases owing to the presence of a unique attracting orbit, the low-Reynolds-number orientational behaviour of the spheroids found by Qi & Luo is the exact opposite of that predicted for a neutrally buoyant spheroid by the analysis in §4, indicating, for instance, that the bifurcating aspect ratio for a prolate spheroid may lie between 1 and 2. We must add, however, that the aforementioned difference between theory and simulation may also be attributed to other factors. To begin with, the lowest Reynolds number at which simulations were carried out for either spheroid is 8, while the theoretical analysis delineated in §4 is strictly valid only in the limit of weak inertial effects ($Re \ll 1$). It is also to be noted that the simulations were carried out in a bounded domain, and as a result, the confinement ratio, defined as the ratio of the distance between the bounding walls to the spheroidal dimension, may play a role in the orientation behaviour observed. To investigate the effects of confinement, Qi & Luo simulated the rotation of a prolate spheroid for three different confinement ratios – 3, 4 and 4.5 – at a Reynolds number of 240 corresponding to a precessing behaviour. Their results showed that the precessing spheroid shifts towards the vorticity axis with decreasing confinement, implying that the boundedness of the domain may again be crucial to the discrepancy between the theoretical and numerical results.

Some of the earliest experimental observations of irreversible motion of moderate-aspect-ratio spheroids (prolate, axis ratio ≈ 2) in simple shear flow appear to be those of Taylor (1923) who used aluminium spheroids suspended in water-glass, a highly concentrated solution of sodium silicate. As discussed by Saffman (1956), the Reynolds numbers in these experiments are $O(10^{-5})$, and fluid inertial effects are consequently too small to account for the experimentally observed time scales for the drift of the spheroids. Virtually all later experimental efforts, with regard to the motion of orientable particles in Newtonian fluids, focus on rods and disks, being mostly restricted to vanishingly small Reynolds numbers; for instance, see Trevelyan & Mason (1951), Karnis, Goldsmith & Mason (1966) and Frattini & Fuller (1986). In the light of this lack of experimental data to confirm the aforementioned theoretical and computational results, it would be of interest to perform controlled experiments investigating the rotations of neutrally buoyant orientable particles

in a small-gap Couette device as a function of their aspect ratio and Reynolds number.

6. Rotation of sedimenting spheroids in simple shear flow

Here, we examine the orientational motion of a spheroid sedimenting in an ambient simple shear flow, again in the limit of a near-unity aspect ratio. As referred to in the introduction, the first effects of inertia both for sedimenting spheroids, and for neutrally buoyant spheroids in simple shear flow, are, in principle, calculable from a regular perturbation of the governing Navier–Stokes equations for small values of the appropriate Reynolds number – $Re_{sed} = Ua/\nu$ for sedimentation, U being the settling velocity, and $Re = \dot{\gamma} a^2/\nu$ for simple shear. Thus, the dominant contributions to the inertial torque in either case are due to stresses associated with the $O(Re_{sed})$ or $O(Re)$ velocity field at distances from the spheroid of order its own size; the singular (outer) regions beyond the inertial screening lengths – aRe_{sed}^{-1} for sedimentation, and $aRe^{-1/2}$ for shear – contribute stresses that are asymptotically smaller in the limit $Re, Re_{sed} \ll 1$. The $O(Re_{sed})/O(Re)$ velocity field may then be obtained from solving the inhomogeneous Stokes equations, the forcing terms being the inertial acceleration, $Re_{sed} \mathrm{D}\boldsymbol{u}_0/\mathrm{D}t$ or $Re\, \mathrm{D}\boldsymbol{u}_0/\mathrm{D}t$, arising from the leading-order Stokes velocity disturbance in either case.

With sedimentation and shear combined, the leading-order inertial torque is still related to the first correction to the Stokes velocity field obtained via a regular perturbation expansion, now valid for distances less than the smaller of the two inertial screening lengths. The inertial acceleration $\mathrm{D}\boldsymbol{u}_0/\mathrm{D}t$ due to the leading-order Stokes velocity field in this case is no longer a superposition of the accelerations associated with sedimentation and shear alone. Owing to its nonlinear nature, one has, for instance, to account for the convection of the Stokes momentum defect in sedimentation by the Stokes shear velocity field and vice versa; in addition, an inertial force arises from unsteadiness of the sedimentation velocity field owing to the shear acting to change the orientation of the settling spheroid. However, these 'cross-terms' do not contribute to the torque since the Stokes velocity fields in sedimentation and shear are, respectively, even and odd functions of the displacement $\boldsymbol{r}$ from the centre of the spheroid. Thus, while the complete velocity field in the coupled problem, including the first inertial correction, is no longer a superposition of the inertial velocity fields in sedimentation and shear alone, the part contributing to the inertial torque may still be obtained by a linear superposition of the respective angular velocities.

We now investigate the three canonical situations where gravity is along the flow, gradient and vorticity axes of simple shear. The case of gravity aligned with the vorticity direction arises in a vertically aligned cylindrical Couette cell. The latter two cases are encountered, for example, in horizontal and vertical channel flows of non-neutrally buoyant particles. The $O(Re_{sed})$ dimensional torque acting on a spheroid characterized by (2.8), and sedimenting in a quiescent fluid, may be obtained from Cox's results (Cox 1965) and, in our notation, is given by

$$\bar{\mathscr{L}}_{sed} = \frac{29\pi}{20} \mu U a^2 (Re_{sed}\epsilon) \sin\eta \cos\eta, \tag{6.1}$$

where η is the angle between the direction of translation and the axis of symmetry $\boldsymbol{p}$, and the sense of the torque is so as to make the orientation transverse to the direction of sedimentation a stable one. In the limit $\epsilon \ll 1$, U may be taken as the Stokes settling velocity of a sphere, and therefore, coincident with the direction of gravity $\mathbf{1}_g$;

thus, $U=(2/9)a^2\Delta\rho g/\mu$, $\Delta\rho$ being the density difference. When non-dimensionalized with the shear rate $\dot{\gamma}$, (6.1) gives

$$\mathscr{L}_{sed}=\frac{29\pi}{20}\frac{\epsilon Re_{sed}^2}{Re}\sin\eta\cos\eta, \tag{6.2}$$

where η is now the angle between $\boldsymbol{p}$ and $\mathbf{1}_g$.

It is convenient to calculate the inertial torque for the coupled problem, while not imposing a restriction on the ratio of particle to fluid densities. In essence, we now account for the effect of sedimentation on the drift coefficient derived in §4 for an arbitrary St/Re. Note that the torque due to sedimentation vanishes for a neutrally buoyant particle, and the resulting orientation dynamics is still identical to that characterized by $\bar{\xi}_n(\theta)$ in §4. Using (4.21), the balance for the combined equatorial angular momentum may now be written as

$$\begin{aligned}
&-\frac{\epsilon St}{4}\left(\frac{8\pi}{15}\right)\cos\theta\sin\theta+\frac{8\pi}{15}St(1-2\epsilon)\frac{d\Omega_{p3}}{dt}\\
&\quad=-8\pi\left(1-\frac{3\epsilon}{5}\right)\Omega_{p3}+8\pi\epsilon E_{12}+\pi\epsilon Re\left(\frac{20}{21}\sin\theta\cos\theta\sin^2\phi\cos^2\phi\right.\\
&\qquad\left.-\frac{18}{35}\sin\theta\cos\theta\cos^4\phi+\frac{154}{105}\sin\theta\cos\theta\sin^4\phi\right)\\
&\qquad+2\epsilon Re\left[-\frac{32\pi}{21}\sin\theta\cos\theta\cos^2\phi+\frac{83\pi}{36}\sin\theta\cos^3\theta\sin^2\phi\cos^2\phi\right.\\
&\qquad-\frac{79\pi}{252}\sin^3\theta\cos\theta\sin^2\phi\cos^2\phi+\frac{83\pi}{72}\sin\theta\cos^2\theta\sin\phi\cos^3\phi\\
&\qquad-\frac{83\pi}{72}\sin\theta\cos^2\theta\sin^3\phi\cos\phi+\frac{599\pi}{504}\sin^3\theta\sin^3\phi\cos\phi\\
&\qquad-\frac{599\pi}{504}\sin^3\theta\sin\phi\cos^3\phi+\frac{\pi}{36}\sin\theta\cos\theta+\frac{2\pi}{15}(\sin\theta\cos\theta\sin^4\phi\\
&\qquad\left.+\sin\theta\cos\theta\sin^2\phi\cos^2\phi)\right]+\mathscr{L}_{sed3},
\end{aligned} \tag{6.3}$$

where, as before, we only look at the '3' component, this being responsible for the drift across Jeffery orbits.

With $\mathbf{1}_g$ aligned in the vorticity direction, the only non-zero component of the sedimentation torque is $\mathscr{L}_3$ given by (6.2) with $\eta=\theta$, causing the orientation vector $\boldsymbol{p}$ to migrate towards the flow–gradient plane; equation (6.3), averaged over a Jeffery cycle, then leads to an equation for the orbit constant of the same general form as (4.23), namely

$$\frac{\mathrm{d}C}{\mathrm{d}t}=(\epsilon Re\bar{\xi}_{s-vort}w)C, \tag{6.4}$$

where the averaged drift coefficient $\bar{\xi}_{s-vort}$ is now given by

$$\bar{\xi}_{s-vort}(\theta)=\left[\frac{St}{60Re}-\frac{4723}{40320}+\frac{55}{672}\cos^2\theta+\frac{29}{160}\left(\frac{Re_{sed}}{Re}\right)^2\right]. \tag{6.5}$$

Thus, provided

$$\frac{Re_{sed}}{Re} \geqslant 2\left(\frac{1423}{29232} - \frac{2St}{87Re}\right)^{1/2}, \tag{6.6}$$

the additional torque due to sedimentation leads to the emergence of a unique neutral orbit, intermediate between the flow–gradient plane and the vorticity axis, and at a polar angle θ_n obtained now by setting $\bar{\xi}_{s-vort}$ equal to zero; here

$$\theta_n = \cos^{-1}\sqrt{\frac{84}{55}\left\{\frac{4723}{5040} - \frac{29}{20}\left(\frac{Re_{sed}}{Re}\right)^2 - \frac{2St}{15Re}\right\}}, \tag{6.7}$$

and is a monotonically increasing function of Re_{sed}. With $Re_{sed} = 0$, (6.7) reduces to (4.27), derived earlier with the neglect of gravitational effects. As before, the neutral orbit is only stable for a prolate spheroid. For the oblate spheroid, the unstable neutral orbit again divides the unit sphere into basins of attraction corresponding to periodic and fixed-point asymptotic states coincident, respectively, with the flow–gradient plane and the vorticity axis.

The condition (6.6) may be reformulated as one that determines the critical value of the particle to fluid density ratio at which the orientation dynamics undergo a bifurcation – a change of attractor for a prolate spheroid, and a change in the basins of attraction for an oblate one. With the equality in (6.6), one obtains a quadratic in the density ratio, which is easily be solved to obtain the critical density ratio as

$$\left(\frac{\rho_p}{\rho_f}\right)_c = \left(1 - \frac{4}{87N^2}\right) + \sqrt{\frac{16}{7569N^4} + \frac{751}{7308N^2}}, \tag{6.8}$$

where $N = (2a\rho_f g)/(9\mu\dot{\gamma})$. For $N \to \infty$, the inertial torque due to sedimentation dominates and $(\rho_p/\rho_f)_c \to 1$, so the bifurcation occurs even for a particle only slightly heavier than the suspending fluid. With $N \to 0$, the change in the orientation dynamics occurs at a density ratio determined only by the balance of particle and fluid inertial forces due to the ambient shear, and is therefore independent of gravity; the critical density ratio in this case was found to be approximately 2.12 in § 4. Thus, for prolate particles heavier than those corresponding to (6.8), the attractor shifts to a neutral orbit with $\theta = \theta_n$ with $0 < \theta_n < \pi/2$, and for heavier oblate ones, a new basin of attraction surrounding the vorticity axis emerges.

With $\mathbf{1}_g$ along the flow and gradient directions, the inertial torque due to sedimentation causes a prolate (oblate) spheroid to again migrate across Jeffery orbits in the direction of decreasing (increasing) orbit constant, and thence, toward the vorticity axis (flow–gradient plane). Thus, a possible bifurcation in the orientation dynamics as a function of the density ratio is contingent on the inertia of the particle itself that, as seen in § 3, drives a prolate (oblate) spheroid towards alignment with the flow–gradient plane (vorticity axis), in opposition now to both the fluid inertial forces due to shear and sedimentation. We also observe that the drift across Jeffery orbits due to the inertial sedimenting torque is weaker for the flow and gradient cases in relation to the vorticity case analysed above, since a component of the torque in either case also modifies the phase relationship along a Jeffery orbit. In fact, with $\mathbf{1}_g$ along the flow axis, the inertial drift due to sedimentation is perpendicular to the Jeffery orbits only for orientations in the flow–vorticity plane ($\phi = 0$); on the other hand, a similar situation for gradient-aligned settling occurs only for $\boldsymbol{p}$ in the gradient–vorticity plane

($\phi = \pi/2$). Therefore, the change in orbit constant resulting from the sedimentation drift in both flow- and gradient-aligned settling contains a phase-dependent factor: $\cos^2\phi$ for the former and $\sin^2\phi$ for the latter. The averaged drift coefficient for either case is given by

$$\bar{\xi}_{s-flow/s-grad}(\theta) = \left[\frac{St}{60Re} - \frac{4723}{40320} + \frac{55}{672}\cos^2\theta - \frac{29}{320}\left(\frac{Re_{sed}}{Re}\right)^2\right] \tag{6.9}$$

where the coefficient of the sedimentation term in (6.9) is smaller than that in (6.5) by a factor of 1/2, this arising from averaging the trigonometric phase factor of $\cos^2\phi$ or $\sin^2\phi$ over a 2π-Jeffery cycle. Since the sedimentation term is now of an opposite sign compared to (6.5), $\xi_{s-flow/s-grad}$ is no longer a monotonically increasing function of the density ratio. One again obtains an expression for the polar angle of a possible neutral orbit by setting (6.9) equal to zero:

$$\theta_n = \cos^{-1}\sqrt{\frac{84}{55}\left\{\frac{4723}{5040} + \frac{29}{40}\left(\frac{Re_{sed}}{Re}\right)^2 - \frac{2St}{15Re}\right\}}. \tag{6.10}$$

This, of course, corresponds to an actual (steady) orbit only if the argument of the square root in (6.10) lies in the interval [0, 1], implying that the bracketed term lies in the interval [0, 55/84]. When expressed in terms of a quadratic equation involving the density ratio, this implies that, for a neutral orbit intermediate between the vorticity axis and the shearing plane to exist, (ρ_p/ρ_f) must lie in either of the open intervals, $((\rho_p/\rho_f)_{c1}, (\rho_p/\rho_f)_{c2})$ or $((\rho_p/\rho_f)_{c3}, (\rho_p/\rho_f)_{c4})$, where

$$\left(\frac{\rho_p}{\rho_f}\right)_{c1} = \left(1 + \frac{8}{87N^2}\right) - \sqrt{\frac{64}{7569N^4} - \frac{751}{3654N^2}}, \tag{6.11}$$

$$\left(\frac{\rho_p}{\rho_f}\right)_{c2} = \left(1 + \frac{8}{87N^2}\right) - \sqrt{\frac{64}{7569N^4} - \frac{4051}{3654N^2}}, \tag{6.12}$$

$$\left(\frac{\rho_p}{\rho_f}\right)_{c3} = \left(1 + \frac{8}{87N^2}\right) + \sqrt{\frac{64}{7569N^4} - \frac{4051}{3654N^2}}, \tag{6.13}$$

$$\left(\frac{\rho_p}{\rho_f}\right)_{c4} = \left(1 + \frac{8}{87N^2}\right) + \sqrt{\frac{64}{7569N^4} - \frac{751}{3654N^2}}. \tag{6.14}$$

Based on figure 8, which depicts the nature of these intervals as a function of increasing N, we make the following observations:

(*a*) In the limit of strong shear, i.e. with $N \ll 1$, one expects the effects of gravity to be unimportant. Thus, the interval $\left((\rho_p/\rho_f)_{c3}, (\rho_p/\rho_f)_{c4}\right)$ goes off to infinity, while the upper and lower limits of the first interval converge, respectively, to 2.12 and 7.028; as seen towards the end of §4, the latter are the values, that, in the absence of gravity, mark the emergence of the neutral orbit (from the vorticity axis) and its merging into the flow–gradient plane, with increasing (ρ_p/ρ_f).

(*b*) For any finite N less than $N_1 = (8/87)(3654/4051)^{1/2}$, the attractor for a prolate spheroid starts off being coincident with the vorticity axis for $(\rho_p/\rho_f) < (\rho_p/\rho_f)_{c1}$. With (ρ_p/ρ_f) increasing beyond $(\rho_p/\rho_f)_{c1}$, the polar angle of the emergent attracting neutral orbit gradually increases from 0 till it equals $\pi/2$ at $(\rho_p/\rho_f) = (\rho_p/\rho_f)_{c2}$, the orbit now coinciding with the flow–gradient plane. The flow–gradient plane

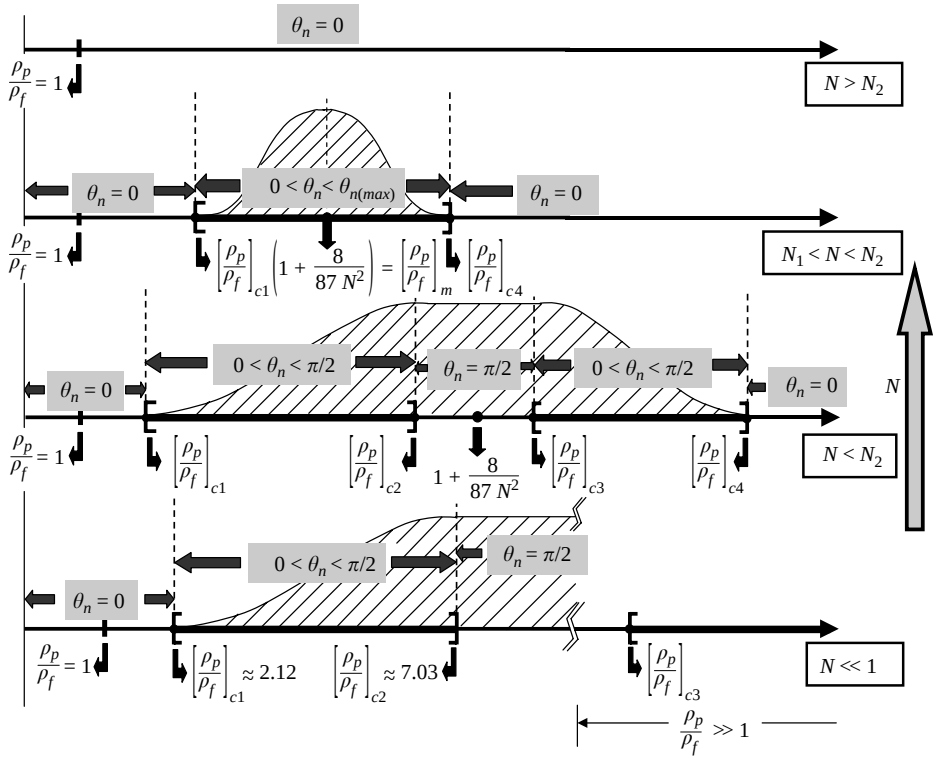

FIGURE 8. The orientation dynamics of a prolate spheroid, as a function of the density ratio, for increasing N, where $N = (2a\rho_f g)/(9\mu\dot{\gamma})$. Schematic (hatched) plots show the variation of the polar angle θ_n of the attractor for each N. Note that the intervals, on the density axis, at different N are not drawn to scale.

remains the attractor in the interval $[(\rho_p/\rho_f)_{c2}, (\rho_p/\rho_f)_{c3}]$. For $(\rho_p/\rho_f) > (\rho_p/\rho_f)_{c3}$, the attractor leaves the shearing plane, and the emergent neutral orbit again tends towards the vorticity axis with increase in the density ratio, becoming coincident with it at $(\rho_p/\rho_f) = (\rho_p/\rho_f)_{c4}$. For all higher density ratios, a prolate spheroid drifts toward the vorticity axis.

(*c*) At $N_1 = (8/87)(3654/4051)^{1/2}$, $(\rho_p/\rho_f)_{c2} = (\rho_p/\rho_f)_{c3}$, so the two intervals, as shown in figure 8, coalesce into one. For $N_1 < N < N_2$, where $N_2 = (8/87)(3654/751)^{1/2}$, the orientation dynamics may be described as follows: at small (ρ_p/ρ_f), the attractor for a prolate spheroid is again coincident with the vorticity axis. For $(\rho_p/\rho_f) > (\rho_p/\rho_f)_{c1}$, a neutral orbit emerges. However, unlike the previous case, the polar angle characterizing the neutral orbit now increases up to a maximum $\theta_{n(max)} < \pi/2$, this being attained at a certain density ratio $(\rho_p/\rho_f)_m$ (say); both these values are, of course, a function of N. Owing to the symmetry of the interval $\left((\rho_p/\rho_f)_{c1}, (\rho_p/\rho_f)_{c3}\right)$ about $1 + (8/87N^2)$, it turns out that $(\rho_p/\rho_f)_m = 1 + (8/87N^2)$, whence one finds

$$\theta_{n(max)} = \cos^{-1}\sqrt{\frac{28}{55}\left\{\frac{4051}{1680} - \frac{8}{435N^2}\right\}}.$$

It is readily verified that $\theta_{n(max)}$ is real-valued and $0 < \theta_{n(max)} < \pi/2$ provided $N_1 < N < N_2$; of course, $\theta_{n(max)} = \pi/2$ for $N = N_1$ and $\theta_{n(max)} = 0$ for $N = N_2$. For

$(\rho_p/\rho_f) > (\rho_p/\rho_f)_m$, θ_n again decreases, and the neutral orbit finally coincides with the vorticity axis at $(\rho_p/\rho_f) = (\rho_p/\rho_f)_{c4}$.

(*d*) At $N_2 = (8/87)(3654/751)^{1/2}$, $(\rho_p/\rho_f)_{c1} = (\rho_p/\rho_f)_{c4}$. For $N > N_2$, none of the critical values (6.11)–(6.14) is real-valued. Thus, the prolate spheroid drifts towards the vorticity axis regardless of the density ratio, this being indicative of the dominant effect of gravity.

For an oblate spheroid, the neutral orbit ($\theta = \theta_n$), when it exists, is always unstable, and thus the bifurcations in its orientation behaviour occur via a qualitative change in the basins of attraction corresponding to the tumbling (flow–gradient plane) and the spinning (vorticity axis) states. For instance, with $N < N_1$, the flow–gradient attractor remains an attractor for all density ratios up to $(\rho_p/\rho_f)_{c1}$, and for all initial orientations except that coincident with the vorticity direction. For density ratios greater than this critical value, a new basin of attraction emerges surrounding the vorticity direction and envelopes the entire unit sphere at $(\rho_p/\rho_f)_{c4}$. The vorticity axis continues to attract all initial orientations (except those in the shearing plane) in the range $[(\rho_p/\rho_f)_{c2}, (\rho_p/\rho_f)_{c2}]$. For $(\rho_p/\rho_f) > (\rho_p/\rho_f)_{c3}$, this basin of attraction starts to shrink until it finally reduces to a point, the intersection of the unit sphere with the vorticity vector, at $(\rho_p/\rho_f) = (\rho_p/\rho_f)_{c4}$. The orientation dynamics remain qualitatively unaltered at higher density ratios.

To summarize, the orientation dynamics of a non-neutrally buoyant spheroidal particle in simple shear, as represented by its trajectories on the unit sphere of orientations, exhibits bifurcations as a function of its density ratio. The nature of the bifurcations depends on the direction of gravity relative to the plane of shear. With gravity along the vorticity axis, the inertial torque due to sedimentation alone, for a prolate spheroid, is consistent with alignment of $\boldsymbol{p}$ with the shearing plane. It is then found, starting from a neutrally buoyant prolate spheroid, that the vorticity axis of simple shear continues to be an attractor for all density ratios up to a critical value given by (6.8); above this value, the attractor moves onto an orbit intermediate between the vorticity axis and the shearing plane, eventually tending toward a tumbling state in the flow–gradient plane. The orientation dynamics therefore remain qualitatively unchanged from that described earlier in § 4 for the absence of gravity. With gravity in the flow and gradient directions, the sedimenting torque acts to move the prolate spheroid in the same direction as fluid inertial forces due to shear. Thus, the vorticity axis ceases to be an attractor only for an intermediate range of densities lying between the values given by (6.11) and (6.14); for density ratios lying in this range, the attractor, as in the vorticity case, is again an orbit lying between the log-rolling and tumbling states, including the flow–gradient plane as a limiting case for density ratios in the sub-interval spanned by (6.12) and (6.13). For an oblate spheroid, the emergent neutral orbit in all the aforementioned cases is unstable, and therefore acts instead to alter the basins of attraction corresponding to the vorticity axis and the flow–gradient plane.

7. Conclusions

In this paper we have analysed the leading-order effect of inertia on the orientation dynamics of prolate and oblate spheroids in simple shear flow, in the limit where the deviation from sphericity is small. In all cases the inertialess degeneracy, entailing an intimate dependence of the long-time orientation distribution on initial conditions, is eliminated. In the absence of gravity, the inertia of the particle and fluid are found to induce opposing torques, the former causing a massive prolate particle to drift toward

the flow–gradient plane. When the density ratio (ρ_p/ρ_f) decreases below 7.028, the attractor shifts onto an intermediate neutral orbit, and finally for density ratios less than about 2.12, inertial forces in the fluid are strong enough to reverse this drift for all initial orientations, and lighter prolate particles, including neutrally buoyant ones, therefore tend toward the vorticity axis.

The inclusion of gravity changes the orientation dynamics in a manner that depends on the relative orientations of gravity and shear. For gravity directed along the vorticity axis, the inertial torque due to sedimentation only acts to enhance the drift already present due to particle inertia, thereby leaving the orientation behaviour qualitatively unchanged. Thus, while the numerical values of the density ratios for its merging with the vorticity axis and the flow–gradient plane change, the attractor continues to move toward the vorticity axis with a decrease in density ratio. Gravity along the flow and gradient axes of simple shear changes the long-time orientation dynamics in a non-trivial manner. For these cases, the axis of a prolate spheroid is again found to range from a tumbling state in the flow–gradient plane, through intermediate precessing states, to an axial spin (log-rolling) about the vorticity axis. The orientation behaviour is, however, complex, with the the long-time dynamics varying in a non-monotonic fashion with the density ratio ρ_p/ρ_f. As illustrated in figure 8, the orientation behaviour now depends both on ρ_p/ρ_f and the shear parameter $N = 2a\rho_f g/(\mu\dot{\gamma})$. For an oblate spheroid, the long-time orientational dynamics correspond to either tumbling or rolling states in all instances, and the relative magnitudes of the shear and sedimenting torques act instead to demarcate the subsets of initial orientations that tend to either state for long times.

In order to illustrate the orientation distributions anticipated in typical shearing flows of non-neutrally buoyant particles, both horizontal and vertical, we consider a few examples:

(*a*) For glass particles ($\rho_p = 2.8\,\mathrm{g\,cm^{-3}}$) of radius 50 microns in air, and with a shear rate of $1\,\mathrm{s^{-1}}$, $St \approx 0.7$, $Re \approx 2.5 \times 10^{-4}$, and $Re_{sed} \approx 0.7$. The value of the shear parameter N is approximately 11, and is much greater than the higher of the two critical values, namely. $N_2 = 0.2028$, so that in horizontal or vertical channel flows of such particulate suspensions, fluid inertia due to shear is negligible and inertial forces due to sedimentation are dominant. According to the classification in § 6, the system then falls in category (*d*), implying that prolate glass particles will exhibit vorticity alignment at sufficiently dilute concentrations.

(*b*) On the other hand, for polystyrene micro-spheres ($\rho_p = 1.05\,\mathrm{g\,cm^{-3}}$) in aqueous media, the inertial torque due to sedimentation is much smaller owing to the small density difference; for spheres with $a = 50$ microns, $Re_{sed} \approx 0.014$. However, since, $(\rho_p/\rho_f) < (\rho_p/\rho_f)_{c1}$ for all shear rates, fluid inertial forces due to shear dominate and prolate particles in channel flows will again align with the vorticity axis.

(*c*) Glass beads suspended in a liquid medium arise in liquid–solid fluidized beds; the latter configuration has recently been used in bio-reactors for microbial sulfate reduction with porous glass micro-beads ($a \approx 100$ microns) being used for the purpose of cell immobilization. Typical values of the fluid density and viscosity may be taken as $\rho_f \approx 1\,\mathrm{g\,cm^{-3}}$ and $\mu \approx 2 \times 10^{-2}\,\mathrm{Pa\,s}$. With $\rho_p \approx 2.5\,\mathrm{g\,cm^{-3}}$, one obtains $Re \approx 5 \times 10^{-4}\dot{\gamma}$, $St \approx 1.3 \times 10^{-3}\dot{\gamma}$, $Re_{sed} \approx 0.01$, and the shear parameter $N \approx 100/(9\dot{\gamma})$ for a characteristic shear rate $\dot{\gamma}$. Therefore, for gravity in the flow or gradient directions, and with $\dot{\gamma} < 55\,\mathrm{s^{-1}}$, the beads again exhibit vorticity alignment. Although N equals the upper critical value N_2 at $\dot{\gamma} \approx 55\,\mathrm{s^{-1}}$, $(\rho_p/\rho_f)_{c4} < 2.5$ at $N = N_2$, so the attractor continues to coincide with the vorticity axis. This is however the case only for a narrow range of shear rates $55\,\mathrm{s^{-1}} < \dot{\gamma} < 63\,\mathrm{s^{-1}}$. For shear rates higher than the

latter value, $(\rho_p/\rho_f)_{c4}$ exceeds 2.5, and the attractor for a prolate glass bead will move onto an intermediate neutral orbit.

(*d*) Finally, transition metal catalysts (rhodium, palladium etc.) supported on alumina ($\rho_p = 3.9\,\mathrm{g\,cm^{-3}}$) are employed, for instance, in the hydrogenation of vegetable oils. For a typical catalyst particle of 100 microns and a low-viscosity oil ($\rho_f \approx 1\,\mathrm{g\,cm^{-3}}$, $\mu \approx 3\times10^{-2}\,\mathrm{Pa\,s}$), one has $Re_{sed} \approx 0.007$; also, $Re \approx 3.33\times10^{-4}\dot{\gamma}$, $St \approx 1.3\times10^{-3}\dot{\gamma}$ and $N \approx 200/(27\dot{\gamma})$. For a shear rate of $200\,\mathrm{s^{-1}}$, $N \approx 0.037 \ll 1$, $(\rho_p/\rho_f)_{c3,c4} > 68$, $(\rho_p/\rho_f)_{c1} \approx 2.13$ and $(\rho_p/\rho_f)_{c2} \approx 7.03$. This implies that prolate catalyst particles, in a horizontal or vertical flow configuration, with $(\rho_p/\rho_f) \approx 3.9$ will, for these shear rates, asymptote toward an intermediate precessing state with a polar angle given by (6.10); this, of course, corresponds to $N \ll 1$ in figure 8. It is also evident from the figure that the density ratio, $(1 + 8/87N^2)$, always corresponds to a tumbling state, independent of N; with a decrease in shear rate, the aforementioned ratio equals 3.9 for $\dot{\gamma} \approx 44\,\mathrm{s^{-1}}$. Correspondingly, the polar angle of the neutral orbit continues to increase with decreasing $\dot{\gamma}$, equalling $\pi/2$ at $\dot{\gamma} \approx 42\,\mathrm{s^{-1}}$. For lower shear rates, the neutral angle now starts decreasing with the neutral orbit coinciding with the vorticity axis at $\dot{\gamma} \approx 37\,\mathrm{s^{-1}}$. For still lower shear rates, prolate particles will continue to align with the vorticity direction as the inertial torque due to gravity becomes dominant.

Previous work accounting for inertial effects in the translation of non-neutrally buoyant spheroids in shear flows have neglected a similar influence on the orientation behaviour. The translation of an orientable particle being coupled to its orientation, the present analysis shows that such a simplistic approach may often lead to incorrect conclusions. For instance, Broday *et al.* (1998) show, for finite St, that the asymmetry of the distribution in phase of a spheroidal particle with respect to the gradient axis, in a vertical shear flow, leads to a lateral migration across streamlines; this is relevant to aerosol depositional processes in turbulent flows. However, in their analysis they constrained the spheroid to execute a tumbling motion in the flow–gradient plane, so the resulting dynamics is effectively two-dimensional. Clearly, both gravity and fluid inertial forces render the tumbling state in this geometry an unstable one, and any deviation from it would therefore lead to a drift toward an asymptotic state of axial spin, that would then act to curtail the lateral migration. It is hoped that our results for the orientational behaviour of spheroidal particles would be taken into account in other similar approaches that examine the motion of non-spherical particles in external flows.

Appendix. The velocity disturbance due to an arbitrarily oriented torque-free spheroid in simple shear flow

Here, we use the results of Chwang & Wu (1975) in order to derive an expression for the Stokes velocity disturbance due to an arbitrarily oriented torque-free spheroid in simple shear flow. The limiting form of the resulting expression, for a small deviation from sphericity, is then used in § 4 to determine the angular velocity of a torque-free neutrally buoyant near-sphere in simple shear flow for small but finite Re.

The velocity-gradient tensor in simple shear, in a coordinate system aligned with the spheroid axis ($\mathbf{1}_1$), is given by

$$\boldsymbol{\Gamma} = \begin{bmatrix} \sin^2\theta\cos\phi\sin\phi & \sin\theta\cos\theta\sin\phi\cos\phi & \sin\theta\cos^2\phi \\ \sin\theta\cos\theta\sin\phi\cos\phi & \cos^2\theta\sin\phi\cos\phi & \cos\theta\cos^2\phi \\ -\sin\theta\sin^2\phi & -\cos\theta\sin^2\phi & -\sin\phi\cos\phi \end{bmatrix} \qquad \text{(A 1)}$$

and has eight independent elements in an incompressible flow. The angles θ and ϕ have been defined in § 3, and we only note that the above coordinate system is chosen with one of its axes ($\mathbf{1}_3$) perpendicular to the vorticity vector, so that $\Gamma_{12} = \Gamma_{21}$, thereby eliminating one of the rotations – the component Ω_{12} of the vorticity tensor. An inertialess torque-free particle in a linear flow, in fact, generates a velocity disturbance only due to the extensional part of the flow. Thus, even the two remaining components of the vorticity tensor (Ω_{23} and Ω_{13}) are rendered superfluous in the calculation of $\boldsymbol{u}'$. We are therefore left with the five independent elements of $\boldsymbol{E}$. Keeping in mind the motions considered by Chwang & Wu (1975), the linear flow relative to the spheroid may then be regarded as a superposition of the following five component flows:

(*a*) Planar extensions in each of two orthogonal planes ($1-3$ and $1-2$) containing the spheroidal axis, with axes oriented at 45° relative to it ($\boldsymbol{u}'_1$ and $\boldsymbol{u}'_2$ below). The velocity disturbance for these cases may be obtained from Chang & Wu by superposing their problems of 'longitudinal shear' and 'cross-flow with longitudinal rate of shear'.

(*b*) Two extensions, both in the equatorial plane ($2-3$) of the spheroid, with principal axes that are at 45° to each other ($\boldsymbol{u}'_3$ and $\boldsymbol{u}'_4$ below). The velocity disturbance for these cases is obtained by a symmetric superposition of 'cross-flows with a transverse rate of shear', again considered by Chang & Wu.

(*c*) An axisymmetric extension with the extensional axis coincident with the spheroidal axis of symmetry ($\boldsymbol{u}'_5$ below).

Stated mathematically, the above amounts to the following decomposition of $\boldsymbol{E}$:

$$
\begin{bmatrix}
\sin^2\theta\cos\phi\sin\phi & \sin\theta\cos\theta\sin\phi\cos\phi & \tfrac{1}{2}\sin\theta(\cos^2\phi-\sin^2\phi) \\
\sin\theta\cos\theta\sin\phi\cos\phi & \cos^2\theta\sin\phi\cos\phi & \tfrac{1}{2}\cos\theta(\cos^2\phi-\sin^2\phi) \\
\tfrac{1}{2}\sin\theta(\cos^{\phi}-\sin^2\phi) & \tfrac{1}{2}\cos\theta(\cos^2\phi-\sin^2\phi) & -\sin\phi\cos\phi
\end{bmatrix}
$$

$$
= \begin{bmatrix}
0 & \sin\theta\cos\theta\sin\phi\cos\phi & 0 \\
\sin\theta\cos\theta\sin\phi\cos\phi & 0 & 0 \\
0 & 0 & 0
\end{bmatrix}
$$

$$
+ \begin{bmatrix}
0 & 0 & \tfrac{1}{2}\sin\theta(\cos^2\phi-\sin^2\phi) \\
0 & 0 & 0 \\
\tfrac{1}{2}\sin\theta(\cos^2\phi-\sin^2\phi) & 0 & 0
\end{bmatrix}
$$

$$
+ \begin{bmatrix}
0 & 0 & 0 \\
0 & 0 & \tfrac{1}{2}\cos\theta(\cos^2\phi-\sin^2\phi) \\
0 & \tfrac{1}{2}\cos\theta(\cos^2\phi-\sin^2\phi) & 0
\end{bmatrix}
$$

$$
+ \begin{bmatrix}
0 & 0 & 0 \\
0 & \tfrac{1}{2}(2-\sin^2\theta)\sin\phi\cos\phi & 0 \\
0 & 0 & -\tfrac{1}{2}(2-\sin^2\theta)\sin\phi\cos\phi
\end{bmatrix}
$$

$$
+ \begin{bmatrix}
\sin^2\theta\sin\phi\cos\phi & 0 & 0 \\
0 & -\tfrac{1}{2}\sin^2\theta\sin\phi\cos\phi & 0 \\
0 & 0 & -\tfrac{1}{2}\sin^2\theta\sin\phi\cos\phi
\end{bmatrix}. \qquad \text{(A 2)}
$$

The velocity disturbance fields corresponding to the above component flows, as derived from Chwang & Wu (1975), are as follows:

$$\boldsymbol{u}_1' = (\sin\theta\cos\theta\sin\phi\cos\phi)\left[\alpha_1\int_{-e}^{e}(e^2-\zeta^2)\boldsymbol{U}_{SS}(\boldsymbol{r}-\boldsymbol{\zeta};\mathbf{1}_1,\mathbf{1}_2)\,\mathrm{d}\zeta + \frac{\beta_1}{2}\int_{-e}^{e}(e^2-\zeta^2)^2\left\{\frac{\partial \boldsymbol{U}_D}{\partial r_1}(\boldsymbol{r}-\boldsymbol{\zeta};\mathbf{1}_2)+\frac{\partial \boldsymbol{U}_D}{\partial r_2}(\boldsymbol{r}-\boldsymbol{\zeta};\mathbf{1}_1)\right\}\right], \quad (A\,3)$$

$$\boldsymbol{u}_2' = \frac{\sin\theta(\cos^2\phi-\sin^2\phi)}{2}\left[\alpha_1\int_{-e}^{e}(e^2-\zeta^2)\boldsymbol{U}_{SS}(\boldsymbol{r}-\boldsymbol{\zeta};\mathbf{1}_1,\mathbf{1}_3)\,\mathrm{d}\zeta + \frac{\beta_1}{2}\int_{-e}^{e}(e^2-\zeta^2)^2\left\{\frac{\partial \boldsymbol{U}_D}{\partial r_1}(\boldsymbol{r}-\boldsymbol{\zeta};\mathbf{1}_3)+\frac{\partial \boldsymbol{U}_D}{\partial r_3}(\boldsymbol{r}-\boldsymbol{\zeta};\mathbf{1}_1)\right\}\right], \quad (A\,4)$$

$$\boldsymbol{u}_3' = \cos\theta(\cos^2\phi-\sin^2\phi)\left[\alpha_2\int_{-e}^{e}(e^2-\zeta^2)\boldsymbol{U}_{SS}(\boldsymbol{r}-\boldsymbol{\zeta};\mathbf{1}_2,\mathbf{1}_3)\,\mathrm{d}\zeta + \frac{\beta_2}{2}\int_{-e}^{e}(e^2-\zeta^2)^2\left\{\frac{\partial \boldsymbol{U}_D}{\partial r_2}(\boldsymbol{r}-\boldsymbol{\zeta};\mathbf{1}_3)+\frac{\partial \boldsymbol{U}_D}{\partial r_3}(\boldsymbol{r}-\boldsymbol{\zeta};\mathbf{1}_2)\right\}\right], \quad (A\,5)$$

$$\boldsymbol{u}_4' = (\sin^2\theta-2)\sin\phi\cos\phi\left[\alpha_2\int_{-e}^{e}(e^2-\zeta^2)\boldsymbol{U}_{SS}(\boldsymbol{r}-\boldsymbol{\zeta};\mathbf{1}_2',\mathbf{1}_3')\,\mathrm{d}\zeta + \frac{\beta_2}{2}\int_{-e}^{e}(e^2-\zeta^2)^2\left\{\frac{\partial \boldsymbol{U}_D}{\partial r_2'}(\boldsymbol{r}-\boldsymbol{\zeta};\mathbf{1}_3')+\frac{\partial \boldsymbol{U}_D}{\partial r_3'}(\boldsymbol{r}-\boldsymbol{\zeta};\mathbf{1}_2')\right\}\right], \quad (A\,6)$$

$$\boldsymbol{u}_5' = \frac{\sin^2\theta\cos\phi\sin\phi}{2}\left[\alpha_3\int_{-e}^{e}(e^2-\zeta^2)\boldsymbol{U}_{SS}(\boldsymbol{r}-\boldsymbol{\zeta};\mathbf{1}_1,\mathbf{1}_1) + \beta_3\int_{-e}^{e}(e^2-\zeta^2)^2\frac{\partial \boldsymbol{U}_D}{\partial r_1}(\boldsymbol{r}-\boldsymbol{\zeta};\mathbf{1}_1)\right], \quad (A\,7)$$

where $\boldsymbol{\zeta}=\zeta\mathbf{1}_1$ is a coordinate along the axis of the spheroid and $2e$ is the inter-focal distance, with the eccentricity e being given by $e=(2\epsilon)^{1/2}$. The constants α_i and β_i are given by

$$\alpha_1 = \frac{e^2\left[-2e(1-2e^2)+(1-e^2)\ln\frac{1+e}{1-e}\right]}{\left[-2e^2+(1+e^2)\ln\frac{1+e}{1-e}\right]\left[2e(2e^2-3)+3(1-e^2)\ln\frac{1+e}{1-e}\right]}, \quad (A\,8)$$

$$\beta_1 = \frac{(1-e^2)\left[-2e^2(1-2e^2)+(1-e^2)\ln\frac{1+e}{1-e}\right]}{8\left[-2e^2+(1+e^2)\ln\frac{1+e}{1-e}\right]\left[2e(2e^2-3)+3(1-e^2)\ln\frac{1+e}{1-e}\right]}, \quad (A\,9)$$

$$\alpha_2 = \frac{2e^2(1-e^2)}{\left[2e(3-5e^2)-3(1-e^2)^2\ln\frac{1+e}{1-e}\right]}, \quad (A\,10)$$

$$\beta_1 = \frac{(1-e^2)^2}{2\left[2e(3-5e^2)-3(1-e^2)^2\ln\frac{1+e}{1-e}\right]}, \quad (A\,11)$$

$$\alpha_3 = \frac{e^2}{\left[6e-(3-e^2)\ln\frac{1+e}{1-e}\right]}, \quad (A\,12)$$

$$\beta_3 = \frac{(1-e^2)}{4\left[6e-(3-e^2)\ln\frac{1+e}{1-e}\right]}, \quad (A\,13)$$

with the unit vectors $\mathbf{1}'_2$ and $\mathbf{1}'_3$, spanning the transverse plane of the spheroid, being defined as $\mathbf{1}'_2 = (\mathbf{1}_2 + \mathbf{1}_3)/\sqrt{2}$ and $\mathbf{1}'_3 = (\mathbf{1}_3 - \mathbf{1}_2)/\sqrt{2}$, respectively. The velocity fields are thus expressed in terms of distributions of the fundamental singular solutions of the Stokes equations along the spheroidal axis: $\boldsymbol{U}_{SS}$ here is the stresslet velocity field representing a straining motion of the liquid, while $\boldsymbol{U}_D$ is the potential doublet. With $[\boldsymbol{a}, \boldsymbol{b}, \boldsymbol{c}]$ being a set of unit vectors, these singular solutions are defined as

$$\boldsymbol{U}_{SS}(\boldsymbol{r}; \boldsymbol{a}, \boldsymbol{b}) = \left[-\frac{\boldsymbol{a}\cdot\boldsymbol{b}}{r^3} + \frac{3(\boldsymbol{a}\cdot\boldsymbol{r})(\boldsymbol{b}\cdot\boldsymbol{r})}{r^5} \right] \boldsymbol{r}, \tag{A 14}$$

$$\boldsymbol{U}_D(\boldsymbol{r}; \boldsymbol{c}) = -\frac{\boldsymbol{c}}{r^3} + \frac{3(\boldsymbol{c}\cdot\boldsymbol{r})\boldsymbol{r}}{r^5}. \tag{A 15}$$

The above singularity solutions were originally derived by Chwang & Wu for the particular case of a prolate spheroid; there does not exist an analogue for an oblate spheroid for finite eccentricity. In the limit $e \to 0$, however, the velocity disturbance due to an oblate spheroid may still be obtained from the above expressions. The limiting velocity fields are, in fact, expansions in e^2 with the leading-order term corresponding to the Stokes velocity field due to a freely rotating sphere in simple shear (see $\boldsymbol{u}'^s$ in (4.2)). The eccentricity e, as defined above, is imaginary for an oblate spheroid, implying that the next term of $O(e^2)$ in the expansion is opposite in sign. Corrections to the Stokes velocity field of a sphere, due to prolate and oblate deviations from sphericity, therefore differ only in sign. This is, of course, also evident from the analysis in § 3 where the spheroid was represented as $r = (1 + \epsilon h)$, the sign of ϵ determining the nature of the spheroid.

In the limit $e \to 0$, the distributions of stresslet and potential quadrupole singularities in the expressions for the velocity fields have only an $O(e)$ spread about the geometric centre $\boldsymbol{r}$ of the spheroid, and one may expand functions of the form $f(\boldsymbol{r} - \zeta \mathbf{1}_1)$ in (A 3) to (A 6) as a Taylor series. Carrying out the expansions and the subsequent integrations, and identifying $e^2/2$ with the shape factor ϵ, one obtains (4.2) with the $\boldsymbol{v}_i$ defined by (4.3)–(4.7).

REFERENCES

Aidun, C. K., Lu, Y. & Ding, E. J. 1998 Direct analysis of particulate suspensions with inertia using the discrete Boltzmann equation. *J. Fluid Mech.* **373**, 287.

Allen, T. A. & Yao-Tsu Wu, T. 1975 Hydromechanics of low-Reynolds number flow. Part 2. Singularity method for Stokes flows. *J. Fluid Mech.* **67**, 787.

Batchelor, G. K. 1970 Slender-body theory for particles of arbitrary cross-section in Stokes flow. *J. Fluid Mech.* **44**, 419.

Bird, R. B., Hassager, O., Armstrong, R. C. & Curtiss, C. F. 1980 *Dynamics of Polymeric Liquids*, Volume 2: *Kinetic Theory*. John Wiley & Sons.

Brenner, H. 1964 The Stokes resistance of a slightly deformed sphere. *Chem. Engng Sci.* **19**, 519.

Bretherton, F. P. 1962 The motion of rigid particles in a shear flow at low Reynolds number. *J. Fluid Mech.* **14**, 284.

Broday, D., Fichman, M., Shapiro, M. & Gutfinger, C. 1998 Motion of spheroidal particles in vertical shear flows. *Phys. Fluids* **10**, 86.

Chwang, A. T. & Wu, T. Y. T. 1975 Hydromechanics of low Reynolds-number flow. Part 2. Singularity method for Stokes flows. *J. Fluid Mech.* **67**, 787.

Cox, R. G. 1965 The steady motion of a particle of arbitrary shape at small Reynolds numbers. *J. Fluid Mech.* **23**, 625.

Ding, E. J. & Aidun, C. K. 2000 The dynamics and scaling law for particles suspended in shear flow with inertia. *J. Fluid Mech.* **423**, 317.

Feng, J., Hu, H. H. & Joseph, D. D. 1994 Direct simulation of initial value problems for the motion of solid bodies in a Newtonian fluid Part 1. Sedimentation. *J. Fluid Mech.* **261**, 95.

Feng, J. & Joseph, D. D. 1995 The unsteady motion of solid bodies in creeping flows. *J. Fluid Mech.* **83**, 102.

Feng, J., Joseph, D. D., Glowinski, R. & Pan, T. W. 1995 A 3-dimensional computation of the force and torque on an ellipsoids settling slowly through a viscoelastic fluid. *J. Fluid Mech.* **283**, 1.

Frattini, P. L. & Fuller, G. G. 1986 Rheo-optical studies of the effect of weak Brownian motion in sheared suspensions. *J. Fluid Mech.* **168**, 119.

Goldstein, H. 1980 *Classical Mechanics*. Addison-Wesley.

Happel, J. & Brenner, H. 1973 *Low Reynolds Number Hydrodynamics*. Noordhoff International.

Hobson, E. W. 1931 *Theory of Spherical and Ellipsoidal Harmonics*. Cambridge University Press.

Huang, P. Y., Feng J. & Joseph, D. D. 1994 The turning couples on an elliptic particle settling in a vertical channel. *J. Fluid Mech.* **271**, 1.

Jeffery, G. B. 1922 The motion of ellipsoidal particles immersed in a viscous fluid. *Proc. R. Soc. Lond.* A **102**, 161.

Kaplun, S. & Lagerstrom, P. A. 1957 Asymptotic expansions of the Navier-Stokes solutions. for small Reynolds numbers. *J. Math. Mech.* **6**, 585.

Karnis, A., Goldsmith, H. L. & Mason, S. G. 1966 The flow of suspensions through tubes.V. Inertial effects. *Can. J. Chem. Engng* **44**, 181.

Kim, S. & Karrila, S. J. 1991 *Microhydrodynamics: Principles and Selected Applications*. Butterworth-Heinemann.

Leal, L. G. 1980 Particle motions in a viscous fluid. *Annu. Rev. Fluid Mech.* **12**, 435.

Leal, L. G. 1992 *Laminar Flow and Convective Transport Processes*. Butterworth-Heineman.

Lin, C. J., Peery, J. H. & Schowalter, W. R. 1970 Simple shear flow around a rigid sphere: inertial effects and suspension rheology. *J. Fluid Mech.* **44**, 1.

MacMillan, W. D. 1960 *Dynamics of Rigid Bodies*. Dover.

Peery, J. H. 1966 Fluid mechanics of rigid and deformable particles in shear flows at low Reynolds numbers. PhD thesis, Princeton University.

Proudman, I. & Pearson, J. 1957 Expansions at small Reynolds numbers for the flow past a sphere and a circular cylinder. *J. Fluid Mech.* **2**, 237.

Qi, D. & Luo, L. 2002 Transitions in rotations of a nonspherical particle in a three-dimensional moderate Reynolds number couette flow. *Phys. Fluids* **14**, 4440.

Qi, D. & Luo, L. 2003 Rotational and orientational behaviour of three-dimensional spheroidal particles in Couette flows. *J. Fluid Mech.* **477**, 201.

Saffman, P. G. 1956 On the motion of small spheroidal particles in a viscous liquid. *J. Fluid Mech.* **1**, 540.

Subramanian, G. & Koch, D. L. 2005 Inertial effects on fibre motion in simple shear flow. *J. Fluid Mech.* **535**, 383–414.

Taylor, G. I. 1923 The motion of ellipsoidal particles in a viscous fluid. *Proc. R. Soc. Lond.* A **103**, 58.

Trevelyan, B. J. & Mason, S. G. 1951 Particle motion in sheared suspensions. I. Rotations. *J. Colloid Sci.* **6**, 354.

Zhang, W. & Stone, H. A. 1998 Oscillatory motions of circular disks and nearly spherical particles in viscous flows. *J. Fluid Mech.* **367**, 329.